

Pliensbachian environmental perturbations and their potential link with volcanic activity: Swiss and British geochemical records

Iris Schöllhorn, Thierry Adatte, Guillaume Charbonnier, Emanuela Mattioli, Jorge Spangenberg, Karl Föllmi

▶ **To cite this version:**

Iris Schöllhorn, Thierry Adatte, Guillaume Charbonnier, Emanuela Mattioli, Jorge Spangenberg, et al.. Pliensbachian environmental perturbations and their potential link with volcanic activity: Swiss and British geochemical records. Sedimentary Geology, 2020, 406, pp.105665. 10.1016/j.sedgeo.2020.105665 . insu-03710127

HAL Id: insu-03710127
https://insu.hal.science/insu-03710127

Submitted on 8 May 2023

HAL is a multi-disciplinary open access archive for the deposit and dissemination of scientific research documents, whether they are published or not. The documents may come from teaching and research institutions in France or abroad, or from public or private research centers.

L'archive ouverte pluridisciplinaire **HAL**, est destinée au dépôt et à la diffusion de documents scientifiques de niveau recherche, publiés ou non, émanant des établissements d'enseignement et de recherche français ou étrangers, des laboratoires publics ou privés.



Distributed under a Creative Commons Attribution - NonCommercial 4.0 International License

Pliensbachian environmental perturbations and their potential link with volcanic activity: Swiss and British geochemical records

Iris Schöllhorn [a,*], Thierry Adatte [a], Guillaume Charbonnier [a], Emanuela Mattioli [b,d], Jorge E. Spangenberg [c], Karl B. Föllmi [a,1]

[a] Institute of Earth Sciences, University of Lausanne, Géopolis, CH-1015 Lausanne, Switzerland
[b] Université de Lyon, UCBL, ENSL, CNRS, LGL-TPE, Villeurbanne 69622, France
[c] Institute of Earth Surface Dynamics, University of Lausanne, Géopolis CH-1015, Switzerland
[d] Institut Universitaire de France, Paris, France

The mechanisms leading to environmental and climate change prior to and anticipating the well-studied Toarcian oceanic anoxic event are not completely understood. Specifically, the role of the continuing break-up of Pangea, associated palaeogeographic rearrangements, and the influence of volcanic activity are less well known. Therefore, we studied the Pliensbachian interval in the open marine, hemipelagic section of the Breggia Gorge in southern Switzerland, to elucidate the potential impact of these major changes on the environment and climate. We identified carbon isotope excursions towards lower values in whole-rock carbonates dated from the Sinemurian/Pliensbachian boundary, *davoei*, *margaritatus*, and *spinatum* Zones, and possibly from the Pliensbachian-Toarcian boundary. Using the whole-rock oxygen isotope record and phosphorus content, we associated these events with phases of increased runoff possibly related to climate warming. We also established the first mercury (Hg) record for the entire Pliensbachian, and in order to verify its validity, we analysed an additional section located along the Dorset coast in southern England. The presence of Hg spikes common in both sections may indicate the influence of episodes of increased volcanic activity. The Hg spike during the earliest Pliensbachian may coincide with a late phase of the central Atlantic magmatic province, and/or increased rifting linked with the opening of the Hispanic corridor. Further significant maxima in Hg contents are observed within the *davoei* and *margaritatus* Zones, and both phases may correspond to early volcanic activity of the Karoo-Ferrar large igneous province. Further analyses are, however, needed to corroborate this interpretation and evaluate the importance of organic-matter scavenging and detrital input in comparison to volcanic activity.

1. Introduction

The Early Jurassic interval witnessed important palaeoceanographic, climate and environmental changes, which were triggered by major tectonic processes leading to palaeogeographic reorganisation, volcanic activity, and associated increases in atmospheric CO_2 (McHone, 1996; Marzoli et al., 1999; Jourdan et al., 2008). The supercontinent Pangaea started to break up during the latest Triassic leading to the opening of the Central Atlantic Ocean. As a consequence, numerous epicontinental basins were formed through "Europe", and seaways opened connecting "Europe" to Panthalassa and the Arctic through the Hispanic Corridor (latest Sinemurian-early Pliensbachian) (Aberhan, 2001; Van de Schootbrugge et al., 2005; Korte and Hesselbo, 2011) and Viking Strait (Early Jurassic, less well dated) (Bjerrum et al., 2001; Surlyk, 2003; van de Schootbrugge et al., 2005). Furthermore, the Central Atlantic Magmatic Province (CAMP), which triggered the mass extinction event at the end of the Triassic, remained active during the Early Jurassic (Cohen et al., 1999, 2004; Cohen and Coe, 2002; Olsen et al., 2003; Whiteside et al., 2007; Kuroda et al., 2010; Rühl et al., 2016). The Karoo-Ferrar Large Igneous Province, which impacted life and the environment during the early Toarcian may have also started earlier during the Pliensbachian (Pankhurst et al., 2000; Jourdan et al., 2008; Caruthers et al., 2014; Ivanov et al., 2017). In addition, carbon storage patterns (Suan et al., 2010; Silva et al., 2011; Caruthers et al., 2014), possibly glacio-eustatic dynamics (Suan et al., 2010; Krencker et al., 2019; Ruebsam et al., 2019), and orbital parameters (Martinez and Dera, 2015; Rühl et al., 2016) modulated the climate changes during this interval.

In this complex and changing world, the Toarcian Oceanic anoxic event (T-OAE ~183 myr), has been extensively studied (e.g., Jenkyns,

* Corresponding author.
E-mail addresses: iris.schoellhorn@unil.ch (I. Schöllhorn), thierry.adatte@unil.ch (T. Adatte), guillaume.charbonnier@unil.ch (G. Charbonnier), emanuela.mattioli@univ-lyon1.fr (E. Mattioli), jorge.spangenberg@unil.ch (J.E. Spangenberg).
[1] Deceased.

1988; Philippe and Thevenard, 1996; Wignall et al., 2005; Fantasia et al., 2018a, 2018b and 2018c; Suan et al., 2018 and references therein). However, an increasing number of studies highlight important climate and environmental changes prior to this event, which remain less well understood, including the Sinemurian-Pliensbachian boundary event, the upper Pliensbachian positive carbon isotopic event (CIE), the end-Pliensbachian *spinatum* negative CIE, and the Pliensbachian-Toarcian boundary event (e.g., Hesselbo et al., 2002; Suan et al., 2008, 2010; Porter et al., 2013; Bodin et al., 2016; Rühl et al., 2016; Bougeault et al., 2017; Peti et al., 2017; Deconinck et al., 2019; Baghli et al., 2020; Mercuzot et al., 2020; Schöllhorn et al., 2020).

We therefore studied the 8.7 Ma Pliensbachian interval (Rühl et al., 2016) prior to the early Toarcian within the lower part of the hemipelagic succession of the Breggia Gorge (Ticino, southern Switzerland, Fig. 1), with the aim to better assess the environmental change during this period and its potential causes (Schöllhorn, 2019). We selected the Breggia section because it constitutes a well-dated hemipelagic/pelagic setting close to the open Tethys Ocean (Fig. 1). We analysed thin sections and performed bulk-rock analyses to study the depositional context. We furthermore studied the carbon-isotope composition to recognise perturbations in the carbon cycle and the oxygen-isotope record, clay mineralogical analyses and phosphorus content, to study the eventual climate and environmental impact.

As volcanic emissions, coal combustion and intrusion-related metamorphism of organic-rich are the largest natural sources of mercury (Hg) in the biosphere (Pyle and Mather, 2003; Pirrone et al., 2010; Sanei et al., 2012; Grasby et al., 2015) Hg measurements have frequently been used to trace phases of intensified volcanism (Sanei et al., 2012; Grasby et al., 2015; Percival et al., 2015; Font et al., 2016; Thibodeau et al., 2016; Fantasia et al., 2018c; Sabatino et al., 2018). We decided therefore in addition to the aforementioned analyses to carry out the first Hg records spanning through the entire Pliensbachian in order to evaluate the occurrence of enrichments and determine their relation to late CAMP and early Karoo-Ferrar volcanic activity. We compared the results obtained on the Breggia section with a record that we measured along the Dorset coast (southern England).

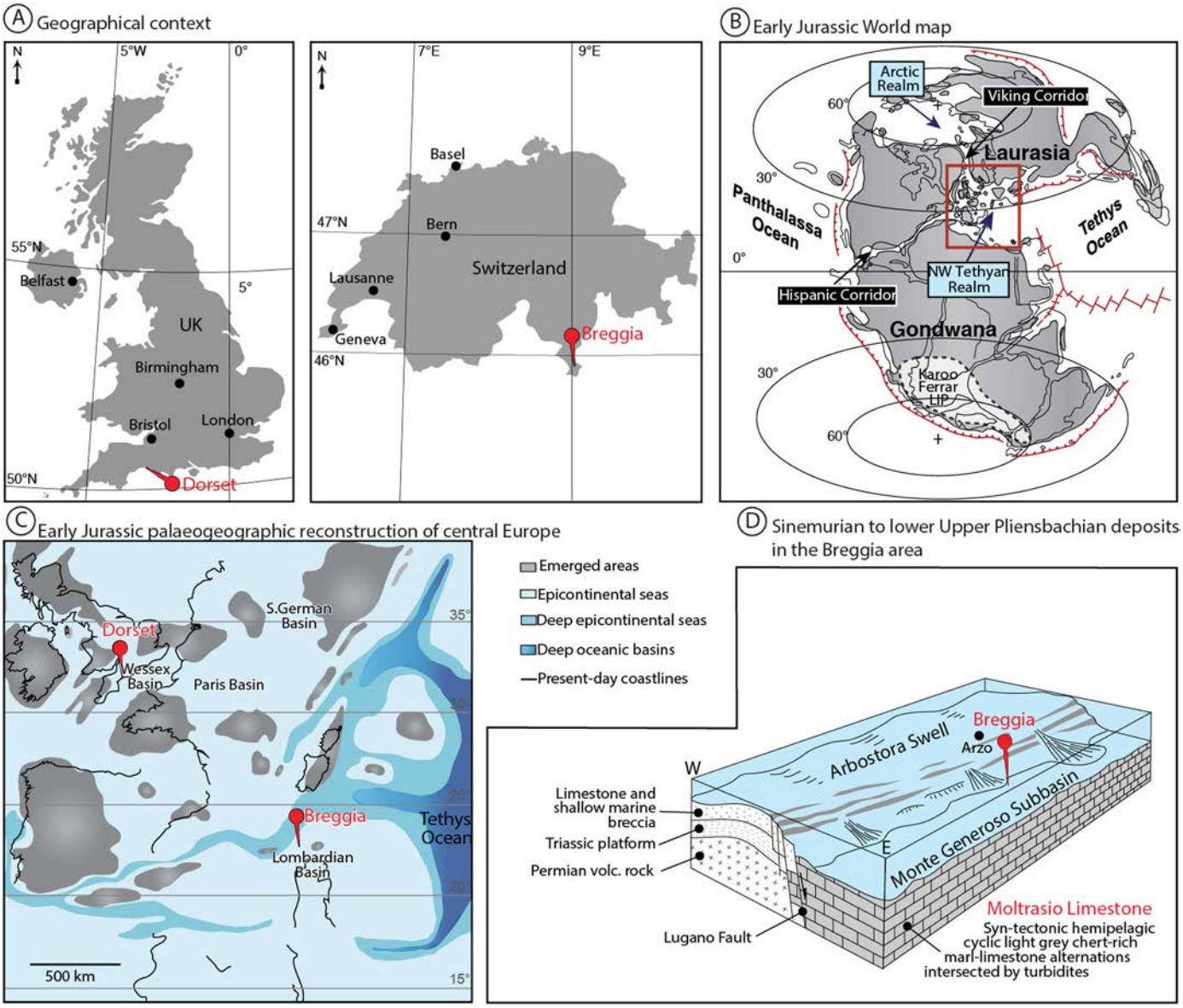


Fig. 1. Geographical context and paleogeographic reconstructions for the Early Jurassic. The World map (B) is from Dera et al. (2011); the central European map (C) is from Thierry (2000) and Fantasia et al. (2018a); the reconstruction of local depositional conditions from the Breggia area is modified from Stockar (2003).

2. Geographical and geological context

2.1. Breggia section

The Breggia section is located in southern Switzerland (Canton Ticino), 16 km to the south of Lugano (45°86′44.78″N, 9°02′11.40″E; Fig. 1). The sediments of this section were deposited in the Lombardian Basin and more particularly in the Monte Generoso Subbasin (Winterer and Bosellini, 1981) along the southern Tethyan passive margin.

The Breggia section has attracted the attention of many geologists because of its continuity (Sinemurian-Cenomanian) (e.g., Stockar, 2003), of deposits characterised by generally elevated sedimentation rates, and the presence of ammonites, which allow for the precise determination of its biostratigraphy (Wiedenmayer, 1980). Horner and Heller (1983) performed a detailed magnetostratigraphic analysis on the Pliensbachian sediments but uncertainties with regards to the calibration of the obtained magnetostratigraphy and correlation of measured lithologies prevented us from using their data.

The Monte Generoso sub-basin was established during the Late Triassic and Early Jurassic, when the shallow-water Adriatic shelf was segmented into highs and half graben by a rifting phase, which led to differential, rapid subsidence (Horner and Heller, 1983; Bernoulli, 1990; Stockar, 2003). The subsidence rate and depth of these complex submarine swells and basins exerted a major control on the sedimentation pattern during the Early Jurassic (Gaetani, 1975; Winterer and Bosellini, 1981; Bertotti et al., 1993; Cobianchi and Picotti, 2001). Relative sea-level change observed in the sediments from the Breggia Gorge resulted therefore from subsidence pattern, and was modulated by general sea-level change and sediment input (Cobianchi and Picotti, 2001).

The Moltrasio Limestone (Pliensbachian; *jamesoni* to middle *margaritatus* Zones(Zs.)) (Wiedenmayer, 1980) is a prominent member of the synrift sedimentary deposits, and is composed of cyclic, hemipelagic, light grey chert-rich marl-limestone alternations (Fig. 2A) (Stockar, 2003). The limestone beds are constituted of micrite and are a few decimetres thick. They regularly include siliceous bands and nodules. The most abundant fossils consist of ammonites, sponge spicules, and crinoids. The biosiliceous and calcareous components are partly of allochtonous origin and transported: siliceous sponges may have colonised the slope of the Arbostora Swell and part of calcareous lime mud has been imported from the adjacent platform (Fig. 1D) (Cobianchi and Picotti, 2001; Stockar, 2003) with a contribution of calcareous sponges and other organisms (external platform) (Keim and Schlager, 1999; Cobianchi and Picotti, 2001). The sediments are often intersected by coarse calci-turbidites, which are due to gravity processes from the Arbostora Swell to the west (Figs. 1D, 2A) (Stockar, 2003). *Thalassinoides* traces occur frequently.

Tectonic activity decreased further near the Pliensbachian-Toarcian boundary, leading to the general, non-differentiated subsidence of swells and basins (Stockar, 2003). The Arbostora Swell became gradually disintegrated and ceased to produce larger amounts of sediments. The conditions became more open-marine and sedimentation more pelagic. This resulted in the rather rapid transition into the deposition of more colourful (red and yellow), nodular, strongly bioturbated marl-limestone alternations (Fig. 2B; Morbio Limestone; late Pliensbachian). The lower sedimentation rates led to high concentrations of fossils including ammonites, nautiloids, belemnites, crinoids, gastropods, brachiopods, bivalves and ostracods (Renz, 1920; Wiedenmayer, 1980).

In the Toarcian, during the onset of the deposition of the Rosso ammonitico Lombardo Formation, tectonic activity ceased. Sedimentation rates further decreased and reached minimal values. Hiatuses were formed such as at the base of the Toarcian leading to the omission of the early part of the Toarcian oceanic anoxic event (T-OAE) (Wiedenmayer, 1980; Fantasia et al., 2018a). The sediments are composed of bioturbated, dominantly red, nodular, thin limestone-marl alternations. High concentrations of ammonites are observed, in addition to nautiloids, belemnites, echinoderm fragments, rare benthic foraminifera, sponge spicules, ostracods, bivalve fragments, shark teeth, perforated intraclasts encrusted by serpulids and silt-sized detrital grains (Renz, 1920; Wiedenmayer, 1980; Fantasia et al., 2018a).

2.2. Dorset

The studied outcrop along the Dorset coast is located between Pinhay Bay and Eype Mouth, near Lyme Regis and Charmouth in southern England (Fig. 1). The ages, ammonite zones (Zs.) and subzones (SZs.), and formations used for the study of the Dorset outcrop were initially published by Hesselbo and Jenkyns (1995). The *aplanatum* and *macdonnelli* Subzones (upper *raricostatum* Z.) and lowermost *jamesoni* Z. are missing (Hesselbo and Jenkyns, 1998; Deconinck et al., 2003; Hesselbo, 2008; Radley, 2008). The origin of these hiatuses is related to the effect of transgression-induced sediment starvation (Hesselbo and Jenkyns, 1998).

The sediments were deposited in the Wessex basin, located in the centre of "European" epicontinental seas. They consist of hemipelagic mudstone with variable proportions of carbonate, marine organic matter and detrital material, which becomes more silty towards the top. This trend was interpreted as the result of a general regression (Hesselbo and Jenkyns, 1995, 1998; Warrington and Ivimey-Cook, 1995).

3. Material and methods

285 samples were collected at a 75-cm average spacing for carbon and oxygen-isotope measurements in the Breggia section. In addition, between 93 and 104 samples were analysed for bulk-rock and clay mineralogy, mercury and phosphorus content. Calcareous nannofossils were studied in 31 samples in selected intervals of the Breggia section in order to add precision on biostratigraphy, and 26 thin sections were prepared. Mercury analyses were performed on 108 samples of the Dorset section. Organic matter content and other geochemical proxies allowing environmental interpretations are provided by Schöllhorn et al. (2020). The analyses and observations were made at the University of Lausanne (Switzerland) with the exception of the nannofossil study, which was carried out at the Université de Lyon (France).

Bulk-rock and clay mineralogy was analysed using a X-TRA Thermo-Arl SCINTAG 2000 diffractometer, following the procedures by Kübler (1983) and Adatte et al. (1996). The whole-rock mineralogy was determined by a semi-quantitative method, using XRD peak intensities of the main minerals compared to external standards (Klug and Alexander, 1974; Kübler, 1983; Adatte et al., 1996). The precision corresponds to 5 wt% for grain minerals and 5 to 10 wt% for phyllosilicates. The clay mineralogy was determined on oriented slides of decarbonated samples and concentrated clay suspensions by XRD (Adatte et al., 1996). Clay-mineral peak positions (2θ; Moore and Reynolds, 1989) were identified on diffractograms of ethylene-glycolated samples for the <2 μm granulometric fraction. The intensities (in CPS) of the clay-mineral peaks were calculated with the WinXRD 2.0–6 ThermoFischer program for a semi-quantitative estimate of the proportion (in relative per cent) of clay minerals.

Preserved organic matter was analysed using a Rock-Eval 6 instrument following the methods described by Behar et al. (2001) and using standard IFP-160000 with an analytical error of <0.1%. We measured total organic-carbon (TOC) content, hydrogen index (HI), oxygen index (OI), and thermal maturity (T_{max}).

Carbon and oxygen stable isotope analyses on whole carbonate rocks were performed using a Thermo Fisher Scientific GasBench II preparation device interfaced with a Thermo Fisher Scientific Delta Plus XL continuous flow isotope ratio mass spectrometer. The isotope ratios were expressed as the per mil (‰) deviation relative to the Vienna Pee Dee Belemnite scale ($\delta^{13}C_{carb}$ and $\delta^{18}O_{carb}$ values as ‰ VPDB). The normalisation of the measured δ-values was performed using international and in-house

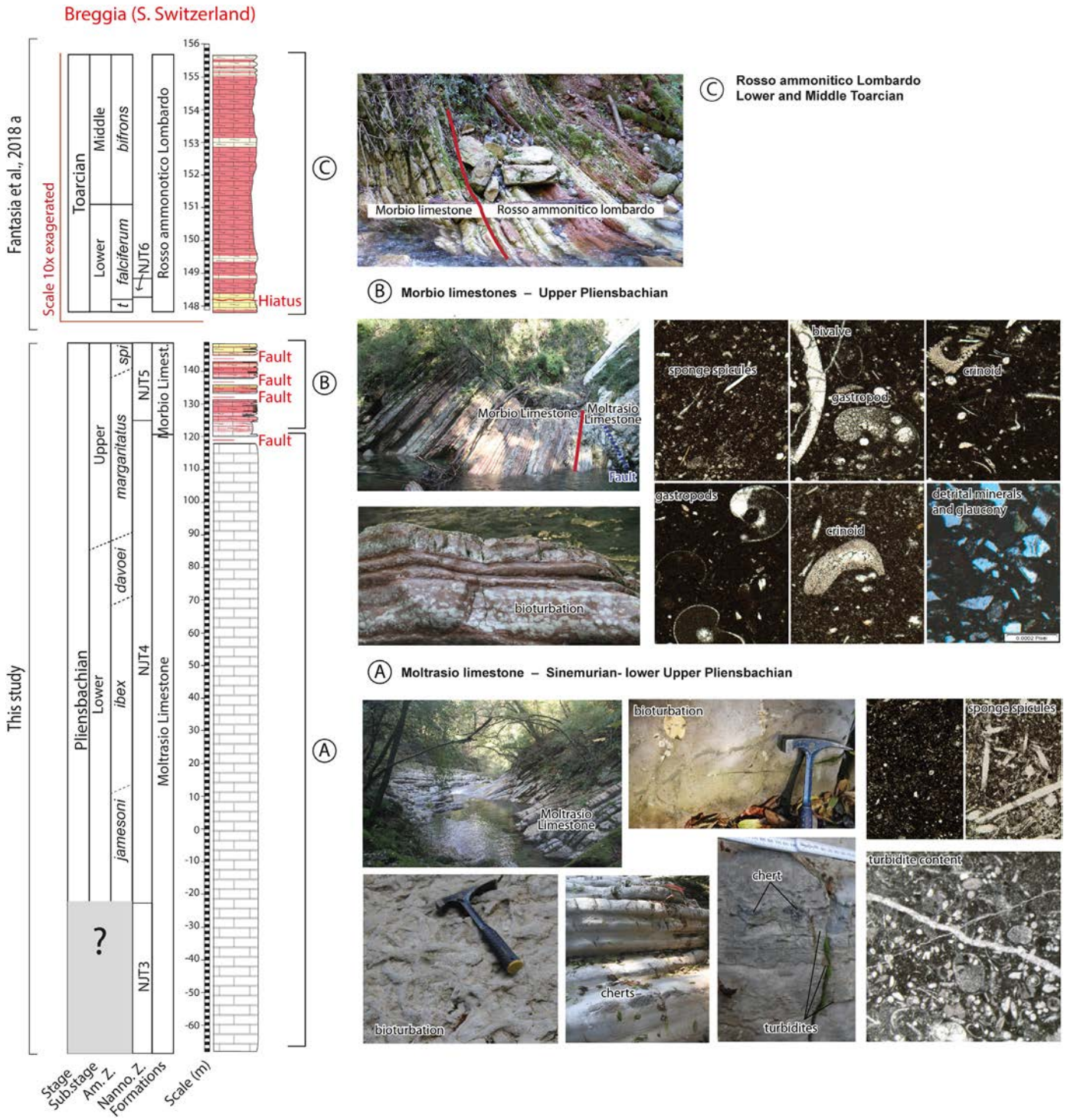


Fig. 2. Formation and facies descriptions along the Breggia section. The ages and formation names are from Wiedenmayer (1980), and the lithological descriptions from the Toarcian are from Fantasia et al. (2018a). (A) Hemipelagic cyclic light grey chert-rich marl-limestone alternations frequently intersected by calciturbidites. The limestone contains ammonites and sponge spicules. (B) Pelagic sedimentation with bioturbated clay-rich, colourful (red and yellow) and nodular marl-limestone alternations with ammonites, crinoids, sponge spicules, gastropods, bivalves, ostracods, and detrital minerals. (C) Pelagic sedimentation with bioturbated, yellow-grey and red nodular marl-limestone alternations with ammonites, echinoderm fragments, rare benthic foraminifera, sponge spicules, ostracods, bivalve fragments, perforated intraclasts encrusted by serpulids, silt-sized detrital grains. For detailed descriptions see Fantasia et al. (2018a). (For interpretation of the references to colour in this figure legend, the reader is referred to the web version of this article.)

Carrara marble standards. Analytical uncertainty (1 σ) is not higher than ±0.05‰ for $\delta^{13}C$ and ±0.1‰ for $\delta^{18}O$.

Total phosphorus measurements were conducted on a UV/Vis Perkin Elmer Lamba 25 spectrophotometer using the ascorbic acid molybdate blue method on whole-rock samples (Eaton, 1995). The concentration of PO_4 (in ppm) is obtained by calibration with internal standard solutions with a precision better than 5%.

Mercury (Hg) analyses were performed on a Zeeman R-915F (Lumex, St-Petersburg, Russia) high frequency atomic absorption spectrometer. Whole-rock powders were measured in the pyrolyser set at Mode 1 (700 °C). Measurements were performed in duplicates and the accuracy was based on certified reference materials (GSD-11 standard, Chinese alluvium: 72 ± 6 ppb) with a correlation coefficient of 0.99 and a standard residual deviation of 0.44. In addition, in marine

and continental settings, Hg is preferentially adsorbed onto organic matter (Benoit et al., 2001; Outridge et al., 2007; Gehrke et al., 2009; Liu et al., 2012; Ruiz and Tomiyasu, 2015) and alternatively onto clays (Krupp, 1988). Therefore, sections containing >0.2% of TOC are normalised by the TOC content.

Microscope slides for nannofossil analysis were prepared using small amounts of powdered rock diluted with water before mechanical spreading onto a cover slide (Bown and Young, 1998). Cover slides were then mounted onto the microscope slide using Rhodopass. The sample slides were then studied using a Leica DM750P optical microscope at 1000 X. At least 300 nannofossils were counted in a variable surface of the slide or, in the nannofossil poor samples, 3 transverses of the slide (9.6 mm) were scanned. The preservation state of the nannofossils was estimated on the basis of the degree of etching and overgrowth, according to Roth (1984).

4. Results

4.1. Breggia section

The geochemical results are described for the Pliensbachian samples. The Toarcian sediments have already been described and interpreted by Fantasia et al. (2018a, 2018b).

4.1.1. Nannofossil content

Nannofossils are in general scarce in the Breggia samples, and some slides are even barren (Table 1). Preservation is commonly very poor and overgrown coccoliths often occur (Fig. 3). However, some productive samples contain zonal markers and allowed us to establish a biostratigraphic scheme. The sample at −22.5 m contains *Similiscutum*. The onset of this genus is commonly observed at the base of the Pliensbachian in strata dated to as *jamesoni* ammonite Zone. This event allows the identification of the NJT4a nannofossil zone (Ferreira et al., 2019) (Fig. 2). The presence of *Lotharingius hauffii* was detected at −22 m. This event allowed us to place the NJT5 zone which correlates with the upper part of the *margaritatus* ammonite zone in several localities (Ferreira et al., 2019). This dating is consistent with ammonite ages for the Breggia section. Finally, the presence of a very overgrown, but still recognisable because of the typical "T" shape in optical microscope (Fig. 3), specimen of *Carinolithus superbus* allows the identification of the NJT6 zone, Early Toarcian.

4.1.2. Mineralogical content

4.1.2.1. Bulk-rock. The bulk-rock mineralogy is mainly (>95 wt%) composed of calcite, quartz, and phyllosilicates (Fig. 4). The remaining part contains K-feldspar, Na-plagioclase, ankerite, dolomite, and unquantified minerals. The light grey Moltrasio limestone (*jamesoni* to early *margaritatus* Zs.) is composed of 9 wt% phyllosilicates on average, and shows a quartz content decreasing from 60 to 20 wt%, and a calcite content increasing from 40 to 70 wt% towards the top. In the *davoei* and *margaritatus* Zs. the phyllosilicate content shows several spikes (at 75, 94, 105 and 116 m), which coincide with higher quartz and lower calcite content. Within the overlying, coloured Morbio limestone (upper *margaritatus* and *spinatum* Zs.) the sediments become richer in carbonate and less siliceous. They are composed of 9 wt% phyllosilicates, 6 wt% quartz, and 82 wt% calcite on average.

4.1.2.2. Clay minerals. The Moltrasio Limestone (lower Pliensbachian to the middle *margaritatus* Z.) is characterised by a low clay content (7% on average). As a result, the low clay contents extracted in the fraction below 2 μm produced spikes close to the background noise, with the exception of illite, which is the most abundant clay mineral. Thus, during the deconvolution process, chlorite, rectorite, smectite, and kaolinite contents were probably exaggerated and even possibly artificially created because of the background effect. They are not further discussed in this paper.

The upper *margaritatus* Z. corresponding to a positive C-isotope shift contains on average 66% smectite and 32% illite, and chlorite and rectorite in negligible amounts (Fig. 5). In sediments of the *spinatum* Z., characterised by a decrease in the C-isotope record, smectite contents decrease (36%), whereas illite contents increase (54%), rectorite contents reach 7%, and chlorite contents go up to 2%.

4.1.3. Organic matter characterisation

Total organic carbon (TOC) is below 0.2 wt% on average with the exception of some samples containing up to 0.42 wt%, which coincide with the negative CIE at the Sinemurian-Pliensbachian boundary between −55 and −25 m (Fig. 5). The hydrogen index (HI) is around 500 mg HC $.g^{-1}$ TOC on average and is not below 274 mg HC $.g^{-1}$ TOC in any sample. The samples containing >0.2 wt% TOC record oxygen indices (OI) of 143 mg CO_2 $.g^{-1}$ TOC on average and a Tmax around 434 °C (Fig. 6). The other samples containing <0.2 wt% TOC record OI 216 mg CO_2 $.g^{-1}$ TOC on average and a Tmax around 452 °C.

4.1.4. Isotope geochemistry

4.1.4.1. $\delta^{13}C_{carb}$. The $\delta^{13}C_{carb}$ values range from −1.2 to 3.1‰ (Fig. 5). The interval of the upper Sinemurian/lower Pliensbachian (−65 m) to lower Pliensbachian (*jamesoni* Z., 6.5 m) records the lowest values throughout the section fluctuating between around −0.7 and 0‰. immediately above, at the top of the *jamesoni* Z., $\delta^{13}C_{carb}$ values increase relatively abruptly to 0.7‰ and then more gradually to 1.9‰ (87 m, *ibex* and *davoei* Zs.). In the sediments corresponding to the lower *davoei* (69 to 77 m) and *margaritatus* Zs. (87 to 115 m), small-amplitude decreases are observed. Then the upper *margaritatus* Z. records a rapid increase from 1.9 to 2.7‰ with the highest values observed at 121.5 m. After that, the $\delta^{13}C_{carb}$ values decrease until 1.5‰ at the top of the *spinatum* Z.

4.1.4.2. $\delta^{18}O_{carb}$. The oxygen-isotope record presents a scattered signal but still shows clear trends correlating well with the $\delta^{13}C_{carb}$ data (Fig. 5). The upper Sinemurian/lower Pliensbachian (−65 m) to lower Pliensbachian (*ibex* Z., 65 m) records the lowest values of around −2.5‰. Then the values increase rapidly up to −1.5‰ and stay stable until the samples of the lowermost *margaritatus* Z. (103 m), where $\delta^{18}O_{carb}$ values increase again to −1‰. The values decrease from the lower *spinatum* Z. (141 m) to the top of the section to −2.3‰.

4.1.5. Phosphorus content

In the Breggia section the phosphorus content varies between 100 and 628 ppm with maximal values recorded at the base of the section within the negative $\delta^{13}C_{carb}$ excursion characterising the *jamesoni* Z. interval (early Pliensbachian) (Fig. 5). High values are also observed within the lower *davoei* Z. (up to 390 ppm), in the lower *margaritatus* Z. (up to 320 ppm), and at the top of the *spinatum* Z. (up to 298 ppm), all three maxima coinciding with negative shifts in the $\delta^{13}C_{carb}$ record. However, it has to be mentioned that the increase recorded within the *davoei* zone is recorded in a small number of samples.

4.1.6. Mercury content

The Hg content ranges from 0.2 to 34 ppb. Three intervals record significantly higher values, which correspond to the *jamesoni* Z. interval (lower Pliensbachian) (up to 34 ppb), the lower *davoei* Z. (up to 29 ppb), and the lower *margaritatus* Z. (up to 17 ppb). They correlate with higher phosphorus contents and negative shifts in the $\delta^{13}C_{carb}$ record (Fig. 5).

4.2. Dorset section

4.2.1. Mercury content

In the Dorset section the mercury content ranges from 4 to 120 ppb. Three intervals record significantly higher values in the *jamesoni* Z.

Table 1
Nannofossils occurrences along the Breggia section.

Sample label	number	depth (cm)	*Schizosphaerella* spp.	*Crucirhabdus primulus*	*Mitrolithus jansae*	*M. elegans*	*M. lenticularis*	*Parhabdolithus robustus*	*P. liasicus liasicus*	*P. liasicus distinctus*	*Parhabdolithus* sp. / *Crepidolithus*	small *Crepidolithus crassus*	*Crepidolithus crassus*	*C. pliensbachensis*	*C. crucifer*	*C. impontus*	small *Tubirhabdus patulus*	*Tubirhabdus patulus*	thin *Calyculus*	large *Calyculus*	*Similiscutum* sp.	large aff. *S. finchii*	*S. finchii*	*S. novum*	*S. avitum*	*S. cruciulus*	*S. orbiculus*	*Discorhabdus ignotus*	*Carinolithus poulnabronei*	*Carinolithus superbus*	*Lotharingius hauffii*	*L. hauffii*	*L. frodoi*	*L. sigillatus*	preservation	Nannofossil zone
BR	20	14927	•	.	•	.	.	.	.	.	.	.	.	.	.	.	.	.	.	.	.	.	.	.	.	.	.	.	.	.	.	.	.	.	VP	NJT6
BR	11	14859	•	.	●	•	•	.	.	.	.	.	•	.	.	•	.	•	.	•	.	.	•	•	●	•	.	•	•	•	•	.	•	.	VP	
BR	8	14834	●	.	●	.	.	.	.	•	.	.	.	.	.	.	.	.	.	.	.	.	.	.	•	.	•	.	.	.	.	.	.	.	VP	NJT5
BR	4	14800	•	.	.	.	.	.	.	.	.	.	.	.	.	.	.	.	.	.	.	.	.	.	.	.	.	.	.	.	.	.	.	.	VP	
BR	1	14784	•	.	.	.	.	.	.	.	.	.	.	.	.	.	.	.	.	.	.	.	.	.	.	.	.	.	.	.	.	.	.	.	VP	
BR	-10	14759	•	.	.	.	.	.	.	.	.	.	.	.	.	.	.	.	.	.	.	.	.	.	.	.	.	.	.	.	.	.	.	.	VP	
BR	-26	14753	•	.	•	.	.	.	.	.	.	.	.	.	.	.	.	.	.	.	.	.	.	.	.	.	.	.	.	.	.	.	.	.	VP	
BR	-51	14728	●	.	•	.	.	.	.	.	.	.	.	.	.	.	.	.	.	.	.	.	.	.	.	.	.	.	.	.	.	.	.	.	VP	
BR	-74	14705	●	.	•	•	•	.	.	.	.	.	•	.	.	.	.	•	.	.	.	•	.	.	.	.	.	.	.	.	.	•	•	•	VP	
BR	-112	14667	•	.	.	.	.	.	.	.	.	.	.	.	.	.	.	.	.	.	.	.	.	.	.	.	.	.	.	.	.	.	.	.	VP	NJT4
BR	-120	14659	•	.	.	.	.	.	.	.	.	.	.	.	.	.	.	.	.	.	.	.	.	.	.	.	.	.	.	.	.	.	.	.	VP	
BRE	214	2048	•	.	.	.	.	.	.	.	.	.	.	.	.	.	.	.	.	.	.	.	.	.	.	.	.	.	.	.	.	.	.	.	VP	
BRE	220	1133,5	•	.	.	•	•	.	.	.	.	.	•	.	.	.	.	.	.	.	.	.	.	.	.	.	.	.	.	.	.	.	.	.	VP	
BRE	221	655	.	.	.	.	.	.	.	.	.	.	.	.	.	.	.	.	.	.	.	.	.	.	.	.	.	.	.	.	.	.	.	.	barren	
BRE	274	-1100	•	.	•	.	.	.	.	.	•	.	.	.	.	.	.	.	.	.	.	.	.	.	.	.	.	.	.	.	.	.	.	.	VP	
BRE	281	-1410	•	.	.	.	.	.	.	.	.	.	.	.	.	.	.	.	.	.	.	.	.	.	.	.	.	.	.	.	.	.	.	.	VP	
BRE	287	-1540	.	.	.	•	.	.	.	.	.	.	.	.	.	.	.	.	.	.	.	.	.	.	.	.	.	.	.	.	.	.	.	.	VP	
BRE	295	-1900	.	.	•	.	•	•	.	.	.	.	•	.	.	.	.	.	.	.	.	.	.	.	.	.	.	.	.	.	.	.	.	.	VP	
BRE	300	-2200	.	.	.	.	.	.	.	•	.	.	.	•	.	.	.	.	.	.	.	.	.	.	.	.	.	.	.	.	.	.	.	.	VP	
BRE	350	-2250	•	.	.	.	.	.	.	.	•	.	.	.	.	.	.	.	.	.	•	.	.	.	.	.	.	.	.	.	.	.	.	.	VP	
BRE	352	-2300	•	•	•	.	•	.	•	.	•	.	•	.	.	.	.	•	.	.	?	.	.	.	.	.	.	.	.	.	.	.	.	.	VP	
BRE	357	-2800	.	.	?	.	.	.	.	.	.	.	.	.	.	.	.	.	.	.	.	.	.	.	.	.	.	.	.	.	.	.	.	.	VP	NJT3
BRE	362	-3600	.	.	.	.	.	.	.	.	.	.	.	.	.	.	.	.	.	.	.	.	.	.	.	.	.	.	.	.	.	.	.	.	barren	
BRE	366	-3700	.	.	•	.	.	.	.	.	.	.	.	.	.	.	.	.	.	.	.	.	.	.	.	.	.	.	.	.	.	.	.	.	VP	
BRE	370	-4100	•	.	•	.	.	.	.	.	.	.	.	.	.	.	.	.	.	.	.	.	.	.	.	.	.	.	.	.	.	.	.	.	VP	
BRE	374	-4500	•	.	•	.	.	.	.	.	.	.	.	.	.	.	.	.	•	.	.	.	.	.	.	.	.	.	.	.	.	.	.	.	VP	
BRE	378	-4900	.	.	.	.	.	.	.	.	.	.	.	.	.	.	.	.	.	.	.	.	.	.	.	.	.	.	.	.	.	.	.	.	barren	
BRE	382	-5300	.	.	.	.	.	.	.	.	.	.	.	.	.	.	.	.	.	.	.	.	.	.	.	.	.	.	.	.	.	.	.	.	barren	
BRE	386	-5700	.	.	.	.	.	.	.	.	.	.	.	.	.	.	.	.	.	.	.	.	.	.	.	.	.	.	.	.	.	.	.	.	barren	
BRE	391	-6100	.	.	.	.	.	.	.	.	.	.	.	.	.	.	.	.	.	.	.	.	.	.	.	.	.	.	.	.	.	.	.	.	barren	
BRE	395	-6500	.	.	•	•	.	•	.	.	•	.	.	.	.	.	•	.	.	.	.	.	.	.	.	.	.	.	.	.	.	.	.	.	VP	

● A: abundant > 1 specimen every 3 field of view
• C: common, 1 specimen in 3-10 fields of view; (16-50)
• F: few, 1 specimen in 15–29 fields of view (6-15)
• R: rare, 1 specimen in 31–150 fields of view (1-5)
. absent
? questionable presence

150 FOV = 1 transverse

Preservation
G = good
M = moderate
P = poor
VP = very poor

(lower Pliensbachian) (up to 120 ppb), in the lower *davoei* Z. (up to 78 ppb) and in the lower *margaritatus* Z. (up to 112 ppb) (Fig. 7).

5. Discussion

5.1. Biostratigraphy of the Breggia section

The Breggia section was precisely dated by ammonites (Wiedenmayer, 1980) and for the uppermost Pliensbachian and Toarcian by nannofossils (Fantasia et al., 2018a). However, the Sinemurian-Pliensbachian boundary is not easily detectable and therefore some additional nannofossil analyses were performed. Nannofossils are scarce in general but one sample at −22.5 m contains *Similiscutum* spp. indicating an early Pliensbachian age (Mattioli and Erba, 1999). Thus the sediments corresponding to the uppermost part of the negative carbon isotope excursion can be correlated to similar records occurring in the *jamesoni* Zone (early Pliensbachian) (e.g., Duarte et al., 2014). A similar correlation between nannofossil biostratigraphy and carbon isotope trend was described by Speranza and Parisi (2007) from the Umbria-Marche Basin in Italy, by Mercuzot et al., 2020 from Morocco and by Ferreira et al. (2019) from the Lusitanian Basin in Portugal.

5.2. Environmental context and bulk-rock mineralogy of the Breggia section

In the Moltrasio Limestone the quartz content measured by XRD consists of a combination of detrital quartz and recristallised biogenic silica as shown by a large peak at 26.6° in XRD diffractograms and by

the presence of chert, extensive silification processes and the large quantities of sponge spicules in thin sections (Fig. 2). However, in most samples the absence of the reflection peaks of the opaline precursor (cristobalite at 21.9°; tridymite at 21.6°) indicates that opal was transformed into α-quartz during diagenesis (Moore and Reynolds, 1989). Only some rare samples are characterised by the presence of opal peaks. The progressive decrease in quartz (60 to 20 wt%) and correspondingly increasing calcite contents (40 to 70 wt%) (Fig. 4) indicate either a decrease in biosilica production, a decrease in detrital quartz input or dilution by increased carbonate production. The generally decrease in sedimentation rate and a diminution in sediment production on the Arbostora Swell (Wiedenmayer, 1980; Stockar, 2003) support the assumption that biosilica production became less important through the Pliensbachian. This may be explained by a general decrease in trophic levels, as would be also indicated by the decrease in P contents and the relative good correlation between quartz and P contents throughout the section. An increased distance to the continents due to the general deepening (Stockar, 2003), may have been a further factor in the decline in silica contribution. However, this cannot be the main factor, as the detrital material is in general scarce.

Near the Pliensbachian-Toarcian boundary the calcite production became highly dominant (82 wt%) and biogenic and detrital quartz became even more scarce (6 wt%) (Fig. 4). This reflects that the tectonic activity decreased further leading to the general, non-differentiated subsidence of swells and basins (Stockar, 2003) and thus to decreased marine sediment production and terrestrial inputs.

Within the Toarcian, during the onset of the deposition of the Rosso ammonitico Lombardo Formation, tectonic activity ceased. Sediment export was minimal on the adjacent Arbostora Swell and biosilica content did not exceed 10 wt% (Fig. 2C) (Fantasia et al., 2018a). The carbonate content decreased during the lower *falciferum* Z., which may have been related to a general biocalcification crisis in pelagic and benthic communities during the T-OAE (Fantasia et al., 2018a). A second decrease in carbonate content is recorded during the uppermost *falciferum* and *bifrons* Zs. (Fig. 4; 58 wt%). During this second phase, relative phyllosilicate contents became high (24 wt%). Based on the high kaolinite content (17% on average) (Deconinck and Bernoulli, 1991; Fantasia et al., 2018b), reflecting an intensification in runoff because of a more humid climate, Deconinck and Bernoulli (1991) proposed that this resulted from increased terrestrial input (Fig. 5). The Toarcian interval may however have recorded a regressive trend (Cobianchi and Picotti, 2001) in this area and therefore the higher kaolinite content registered in sediments of the upper *falciferum* Z. upwards may be related in part to a return to a shallower depositional setting, more favourable to the accumulation of kaolinite.

5.3. Carbon isotope perturbations

Several carbon cycle perturbations affecting the environmental and climate conditions occurred during the Early Jurassic (Fig. 8) (Table 2). However, few records (Gröcke et al., 2011; Baghli et al., 2020; Mercuzot et al., 2020) have been obtained from sections located outside epicontinental European Basins. This study on the Breggia Gorge evaluates their relevance in a setting close to the open Tethys. The $\delta^{13}C$ data vary between −1 and 4‰ (Fig. 5) and burial depth did not exceed 2000 m (Deconinck and Bernoulli, 1991). This indicates that there is no clue for a diagenetic overprint. However, as the $\delta^{13}C$ was measured on bulk carbonate and as changes within the carbonate producers occurred within the Lombardian Basin (see part 5.2), the carbon isotope signal from bulk carbonate may have varied as a function of carbonate producers. The general trends are therefore compared to those detected in other sections.

The uppermost Sinemurian-lowermost Pliensbachian interval records the lowest values throughout the section, fluctuating between −0.7 and 0‰ (Fig. 5). They increase at the end of the *jamesoni-ibex* Zs. The onset of this negative excursion was not observed because of the inaccessibility of the section. A coeval negative carbon isotope excursion (CIE) has been recorded in basins in Spain, Portugal, Italy, Algeria, Morocco, England, France, and Canada in organic matter, bulk carbonate, belemnites, and other calcitic organisms (Fig. 8) (Table 2 for references). Its widespread distribution provides good evidence for the importance of the CIE, which may have resulted from changes in the carbon cycle on a global scale.

Following the Sinemurian-Pliensbachian negative CIE, the trend to higher values recorded from the lower to the upper Pliensbachian (*ibex* to *margaritatus* Zs.) culminates to a maximum in the *subnodosus* SZ. (*margaritatus* Z.) (Fig. 5). This general trend was also recorded from sections in England, Portugal, Spain, France, Italy, Algeria, Morocco western Canada, and northern Alaska, on organic matter, wood, bulk carbonate, belemnites, and other calcitic organisms (Fig. 8) (Table 2 for references).

Superimposed on this long-term trend, two small negative excursions were recorded in the Breggia section in sediments corresponding to the *davoei* Z. and the lowermost *margaritatus* Z. (Fig. 5). A negative trend in the *davoei* Z. was also documented in sections from Portugal, Italy, Canada, England, Morocco and France on organic matter and bulk carbonate (Fig. 8) (Table 2 for references). The negative *margaritatus* Z. CIE may coincide with the one recorded in sections in Portugal, Canada, France, England, Spain, Morocco, Italy and Chile measured on bulk carbonate, organic matter and belemnites (Fig. 8) (Table 2 for references).

The upper Pliensbachian sediments from the Breggia section (*spinatum* Z.) are characterised by a negative shift of around 2‰, which is also detected in sections in France, Spain, Portugal, the Carpathians, and the UK on organic matter, wood, bulk carbonate, belemnites, and other calcitic organisms (Figs. 5, 8) (Table 2 for references).

An additional negative CIE is recorded around the Pliensbachian-Toarcian boundary (Fig. 5) in sections from Morocco, UK, Italy, Algeria, Poland, Japan, Luxembourg, and Portugal on organic matter, wood, bulk carbonate, belemnites and other calcitic organisms (Table 2 for references). In the Breggia section this event is possibly recorded in sediments near the top of the *spinatum* Z. (Upper Pliensbachian) or directly following the Pliensbachian-Toarcian boundary. However, as hiatuses are reported near the Pliensbachian/Toarcian boundary, it seems difficult to correctly document this event for this locality.

5.4. Environmental and climate perturbations

5.4.1. Phosphorus content

In the Breggia section, the phosphorus background content is around 150 ppm. P enrichments above background level were recorded in sediments corresponding to the Sinemurian-Pliensbachian boundary (*jamesoni* Z.; up to 680 ppm), the lower *davoei* Z. (up to 390 ppm), the lower *margaritatus* Z. (up to 320 ppm), and the top of the *spinatum* Z. (up to 298 ppm) (Fig. 5). All these enrichments do not only coincide with negative shifts in $\delta^{13}C_{carb}$ but also for some of them with high Hg contents (Fig. 5). Increases in the P content in this setting may be explained by:

(a) Changes in redox conditions with oxygen depletion leading to the remobilisation of P in the sediments.
(b) Decreased sedimentation rates allowing more dissolved seawater P to be precipitated or adsorbed within sediments.
(c) Intensified upwelling leading to the delivery of larger amounts of nutrients.
(d) Increased input of P into the basin related to intensified (bio) chemical weathering on the continent and/or increased aeolian input.

Oxic conditions remained steady throughout the entire section, as shown by the omnipresence of bioturbation (Fig. 2). The occurrence of

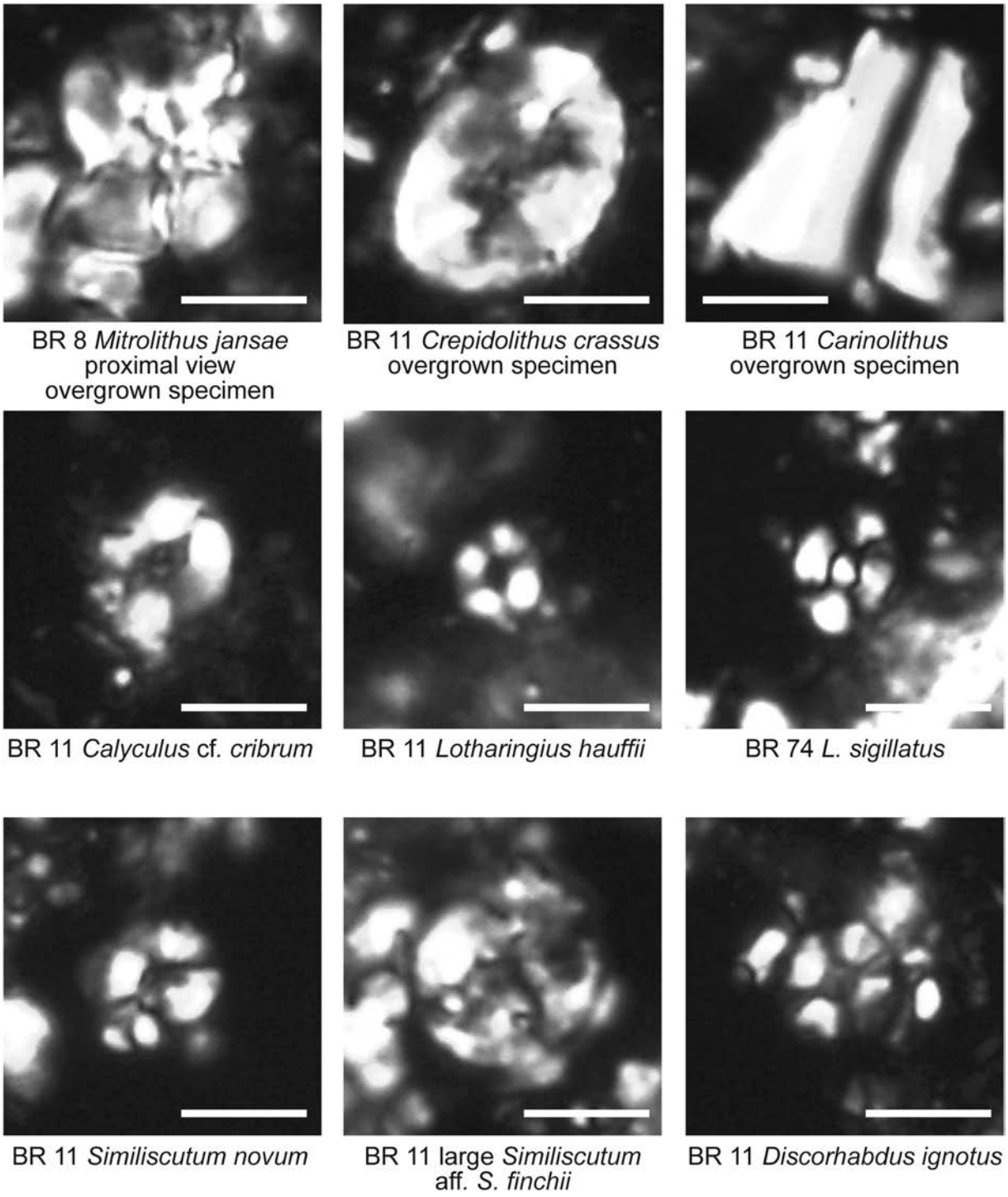


Fig. 3. Pictures of some biostratigraphically relevant species recorded in the Breggia section, with sample label. Pictures also show the overall poor preservation state of coccoliths. *Mitrolithus jansae* are often observed as extremely overgowth specimens in proximal view. These specimens closely resemble the forms reported by Casellato and Erba (2015) as *Rucinolithus* sp. from a similar stratigraphic interval in the Colle di Sogno section (their Figs. 16, 17). *Carinolithus superbus* is also extremely overgrown, but the typical «T» shape allows us to discriminate it from *C. poulnabronei* (typically represented by a «V» shape in side view).

Thalassinoides may partly be related to turbidite deposition, which may have assisted in oxygen supply to the deeper waters (Föllmi and Grimm, 1990). The changes in P are therefore unlikely to be due to changes in redox conditions (a). Neither is the P content related to decreased sedimentation rates (b). The sedimentation rate decreased significantly from the upper *margaritatus* Z. up to the Toarcian, but this pattern is not reflected in the background P content, which also shows an overall decreasing trend. In addition, the P-rich samples do not coincide with the presence of hardgrounds, glaucony, and other sign of condensation. Enhanced upwelling (c) is unlikely, because this would lead to oxygen depletion, changes in ecosystems and a possible increase in preserved organic matter which are not observed at Breggia. The quartz record (Fig. 4) which is likely mainly biogenic in origin shows a long-term trend, which appears rather well correlated with the long-term trend in P contents. Therefore, the most likely explanation is that (d) the intervals with high P levels are related to increased P input into the basin

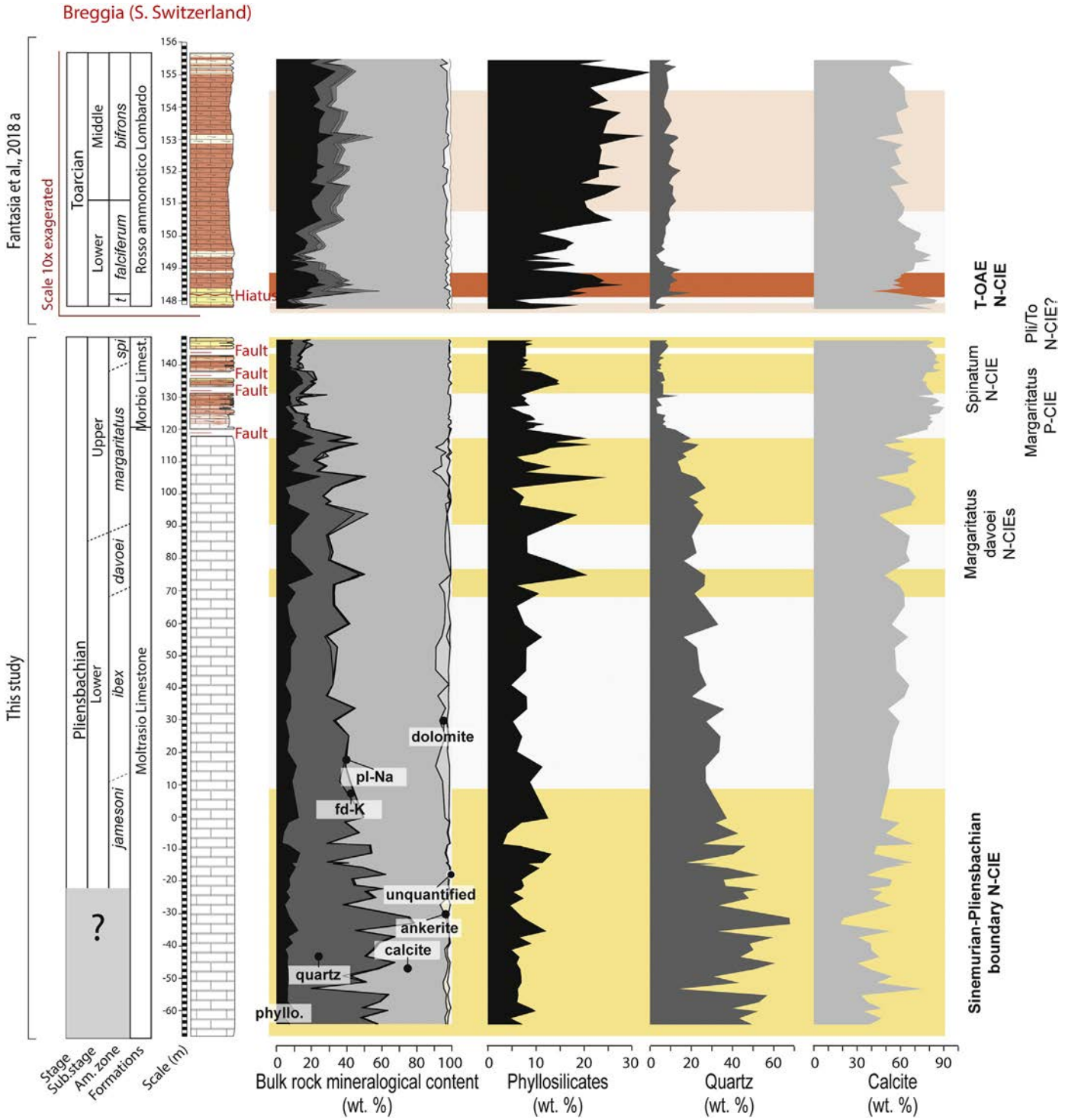


Fig. 4. Bulk mineralogical content from the Breggia section. Pl-Na = Na plagioclase; Fd-K = K feldspar; P = positive; N = negative; CIE = carbon isotope excursion. Data from the Toarcian are from Fantasia et al. (2018a, 2018b).

associated with changes in the climate towards warmer and more humid conditions on the adjacent continent, inducing higher weathering and mobilisation rates of P and Silica (Si). Interestingly, P contents are high in those sediments for which general accumulation rates were high as well, which shows that there might be a general relation between P availability and Si and $CaCO_3$ production.

5.4.2. $\delta^{18}O$

An analysis of bulk-rock oxygen isotopes had already been performed by Jenkyns and Clayton (1986), on the higher part of the same section, from the *ibex* Z. (Pliensbachian) to the Toarcian. Their results are comparable to ours, and the trends are the same (Fig. 5). Jenkyns and Clayton (1986) interpreted their $\delta^{18}O$ record as reflecting diagenesis based on the non-negligible correlation between carbon and oxygen isotopes. Indeed, the cross plot between oxygen and carbon isotopes indicates a correlation with R^2 between 0.29 and 0.45 depending on the formations (Fig. 9). However, the oxygen isotope record does not correlate significantly with the calcite content (R^2 between 0.03 and 0.15) and neither with lithological change (Fig. 9). Furthermore, more negative $\delta^{18}O$ values coincide with increased P content and Hg enrichments

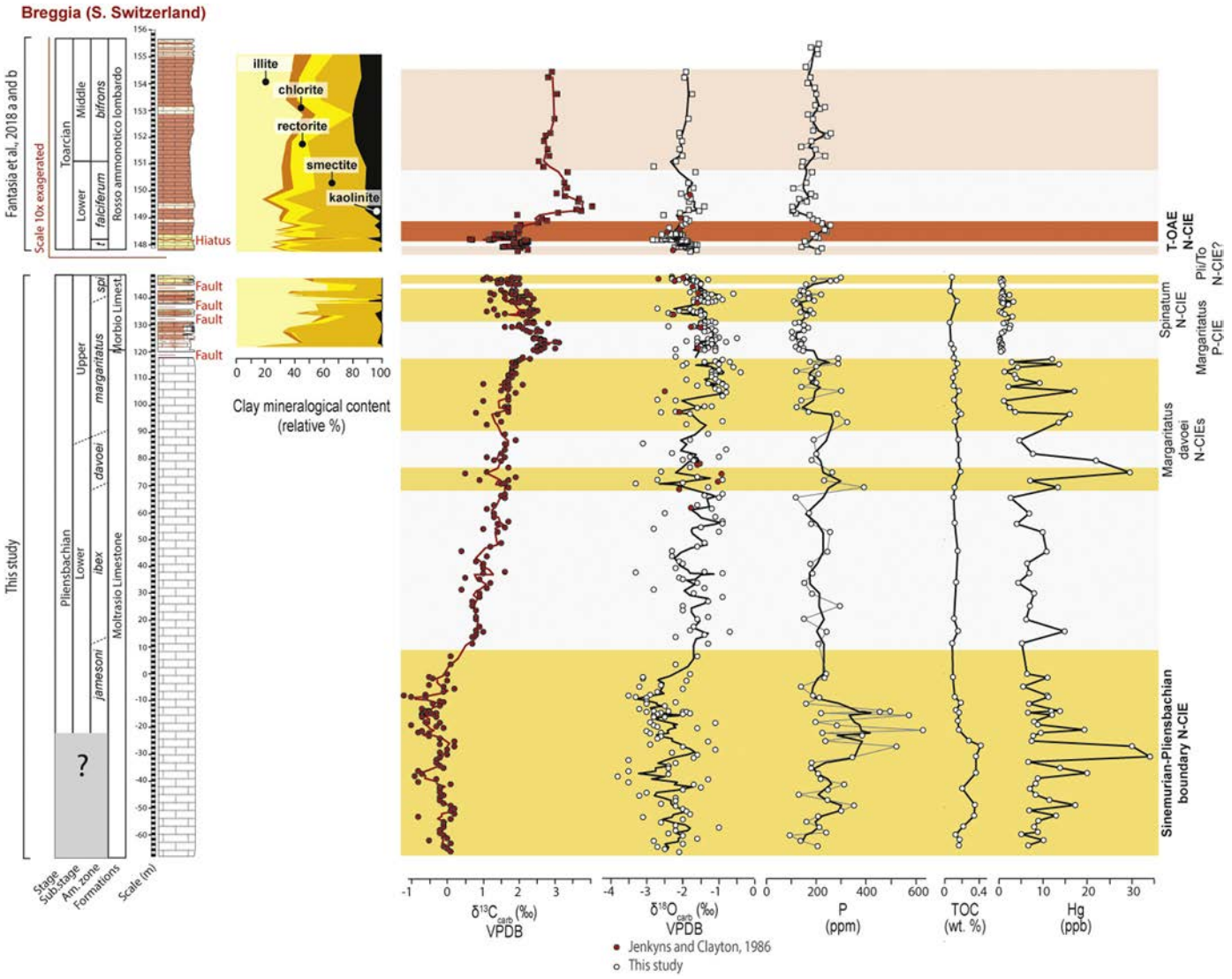


Fig. 5. Geochemical data along the Breggia section. Clay mineralogical content, stable carbon and oxygen isotopes performed on bulk carbonate ($\delta^{13}C_{carb}$ and $\delta^{18}O_{carb}$), phosphorus content (P) and mercury content (Hg). P = positive; N = negative; CIE = carbon isotope excursion. Data from the Toarcian are from Fantasia et al. (2018a, 2018b).

during the Sinemurian-Pliensbachian negative CIE (Fig. 5). This coincidence is not thought to have resulted from diagenesis alone and underlines the possible impact of environmental change on the oxygen isotope record. The short-term scattering in the $\delta^{18}O$ values is, however, likely explained by diagenetic overprint.

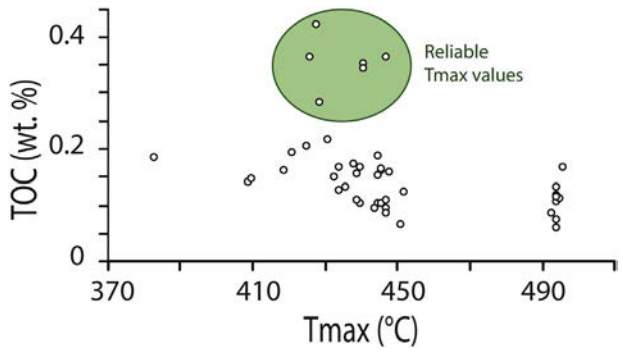


Fig. 6. Cross-plot between T max (themal maturity) and TOC (total organic carbon) along the Breggia section.

5.4.3. Mineralogical clay content of the Breggia section

Deconinck and Bernoulli (1991) demonstrated that the burial depth did not exceed 2000 m in the Breggia area based on the abundance of smectite and the illite cristallinity index (Kübler, 1964). They suggested that therefore, the clay mineralogy reflects the original assemblages in the sediments. In the upper Pliensbachian succession (*margaritatus* and *spinatum* zones), it is mainly composed of illite and smectite with fluctuating quantities along the section, in addition to chlorite, rectorite and kaolinite, which occur in lower quantities.

Within the Morbio Limestone the sediments dated from the *spinatum* Z. contain less smectite compared to sediments from the uppermost *margaritatus* Z. (Fig. 5). This decrease in smectite may coincide with a short-term regression phase (Cobianchi and Picotti, 2001; Bougeault et al., 2017). Therefore, the lower smectite content and coeval increase of illite may reflect the decreasing distance to the continent and also a stronger mechanical weathering due to a low sea level. Indeed, because of its settling characteristics smectite can be transported over wider distances than illite (Gibbs, 1967; Godet et al., 2008). However, the decrease in smectite content may also be the result of climate change and would as such indicate a change towards drier conditions. Unfortunately, the uncertainties in the interpretation of the clay mineral

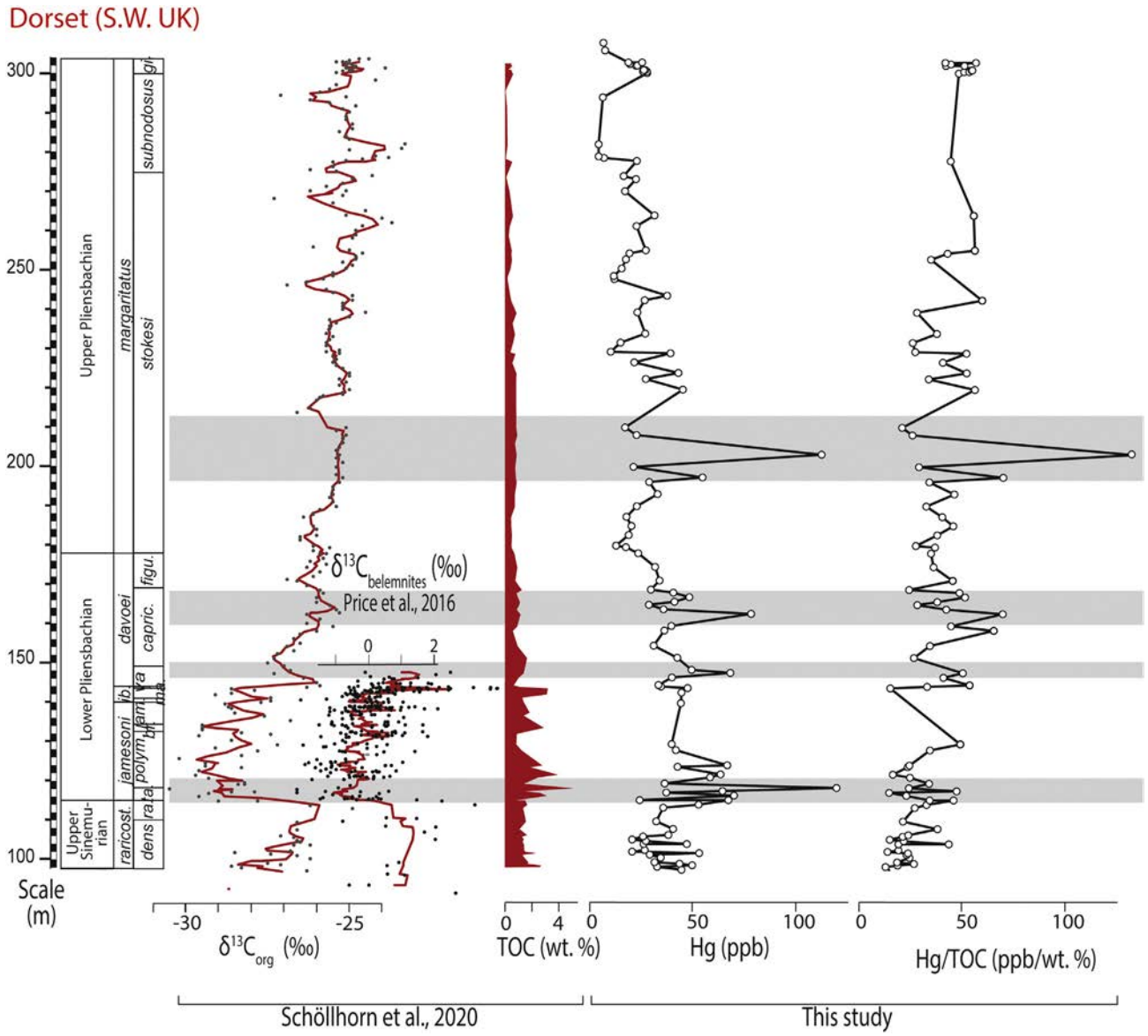


Fig. 7. Geochemical analysis on the Dorset section along the Pliensbachian. Carbon isotope data obtained from organic matter ($\delta^{13}C_{org}$; Schöllhorn et al., 2020) and from belemnites (Price et al., 2016); organic matter content (TOC), Hg content corrected for organic matter content (Hg/TOC) are shown.

composition in the remainder of the section do not allow its use for any further palaeoclimate evaluation.

5.4.4. Organic matter content

The total organic carbon (TOC) is below 0.2 wt% on average with the exception of some samples containing up to 0.42 wt% coinciding with the negative CIE at the Sinemurian-Pliensbachian boundary. The organic matter within these samples is dominated by marine components as suggested by the high HI values (380 HC $.g^{-1}$ TOC) (Espitalié, 1986; Espitalie et al., 1986). This pattern may express a certain rise in marine organic productivity, which would be coherent with the increase in nutrient influx as shown by the increase in P content and a warmer and/or more humid climate as evidenced by the $\delta^{18}O$ record near the Sinemurian-Pliensbachian boundary. The organic matter within the samples containing higher TOC contents is immature (Tmax = 434 °C) and not as much altered (OI = 143 mg CO_2 $.g^{-1}$ TOC) (Espitalié, 1986; Espitalie et al., 1986) (Fig. 6). In contrary organic matter within the other samples containing <0.2 wt% of TOC records higher and not trustworthy OI and Tmax values (OI = 216 mg CO_2 $.g^{-1}$ TOC; Tmax = 452 °C) (Espitalié, 1986; Espitalie et al., 1986). This is related to the fact that the Rock-Eval analysis becomes less reliable below a threshold of 0.2–0.3 wt% TOC or to the presence of much more altered and mature organic matter residing in the samples with low TOC (Espitalié, 1986; Espitalie et al., 1986) (Fig. 6). The entire series is thusly considered as immature.

5.4.5. Comparison with global climate records

5.4.5.1. The negative CIE near the Sinemurian-Pliensbachian boundary. A trend to lower values in the oxygen isotope data recorded during the negative CIE near the Sinemurian-Pliensbachian boundary was also observed in the Umbria Marche Basin (Fig. 10; Italy) (Speranza and Parisi, 2007). A similar diagenetic evolution for both sections is unlikely and therefore supports either an environmental origin meaning an increase in temperature or a change within the carbonate content. The nature of the bulk carbonate in Early Jurassic sediments is essentially unknown but as nannofossils tend to occur rarely at that time, it is likely that the source of the carbonate is not dominantly pelagic. Hence, micritic

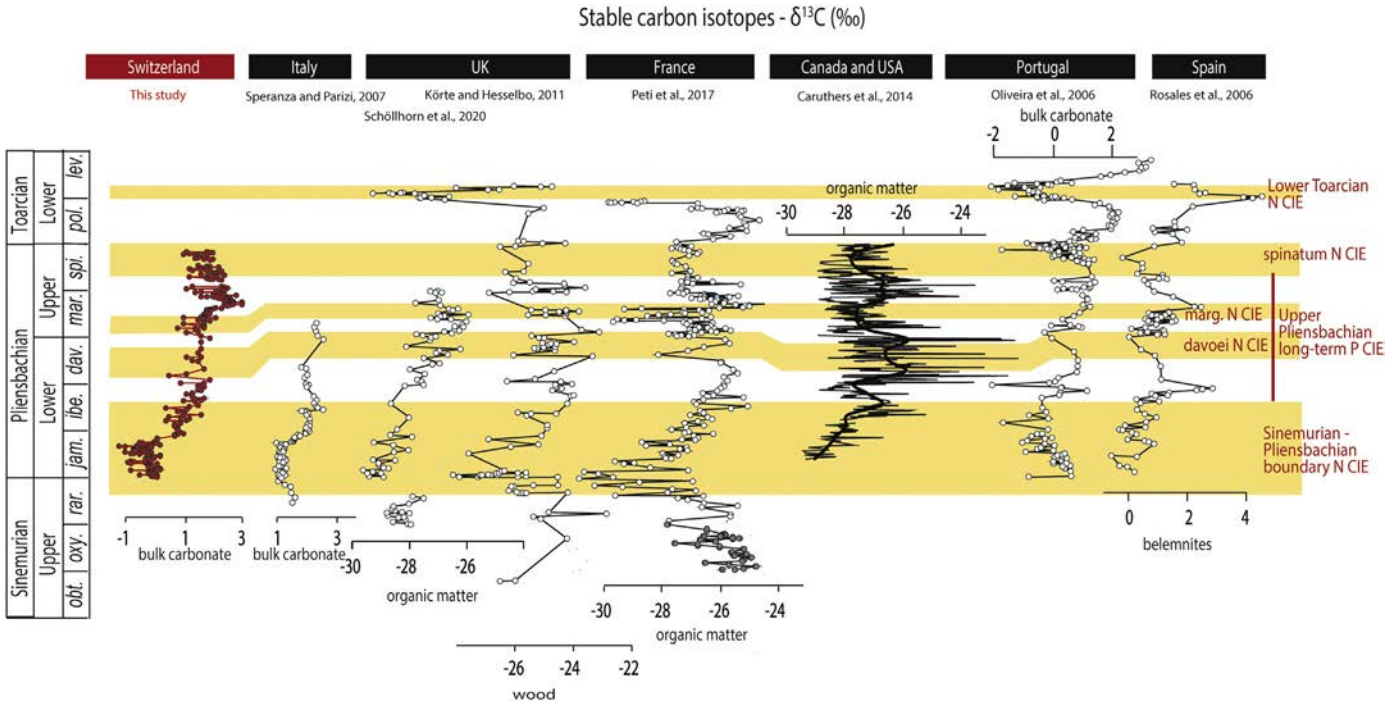


Fig. 8. Compilation of carbon isotope ($\delta^{13}C$) records from different basins along the Pliensbachian interval.

carbonate was probably essentially sourced from platform carbonates detritus at that time, which by nature is very heterogeneous and susceptible to changes in the composition of organisms that produced this carbonate over time, following climate and sea level changes. Environmental interpretations based on bulk records alone are therefore difficult and have to be compared to further climate proxies.

Evidence for global warming and/or increased fresh water inputs may be given by lower $\delta^{18}O$ values in the Lusitanian Basin (Portugal) (Suan et al., 2010; Ferreira et al., 2019) and Algeria (Baghli et al., 2020). More humid conditions are supported by an increased kaolinite content in the southern Paris (France), Cardigan Bay and Cleveland (United Kingdom) Basins (van Buchem et al., 1992; Bougeault et al., 2017; Deconinck et al., 2019) (Fig. 10). However, the increase in kaolinite across the S/P in the Sancerre core (France) (Bougeault et al., 2017) is very small and the kaolinite content remains much lower than it is in the upper Pliensbachian. Additional evidence was provided from the eastern margin of Gondwana (Pakistan) (Iqbal et al., 2019), at that time in the southern hemisphere (Fig. 10). This evidence is based on an increase in the chemical alteration index and in kaolinite contents around the Sinemurian-Pliensbachian boundary. However, this is based on two samples only, and further research is needed to substantiate their results. Warmer, more humid climate during the negative Sinemurian-Pliensbachian boundary CIE may as such explain the lower $\delta^{18}O$ values and the higher P input rates observed in the Breggia section.

In contrast, higher $\delta^{18}O$ values (Fig. 11) that could indicate a cooling event and/or a decrease in the fresh water inputs were recorded in the Asturian Basin (Spain) (Gómez et al., 2016), in the Basque Cantabrian Basin (Spain) (Rosales et al., 2004a, 2004b), in the Cleveland Basin (UK) (Korte and Hesselbo, 2011) and in the Wessex Basin (UK) (Price et al., 2016; Schöllhorn et al., 2020). Furthermore, Peti and Thibault (2017) reported a transient shift in size of *Schizosphaerella* towards the warm-water small morphotypes in the recovery part of the CIE across the *jamesoni* to *ibex* Zs. In the Basque-Cantabrian Basin (Spain), Van de Schootbrugge et al. (2005) recorded a negative shift in the $\delta^{18}O$ record, sustained by a positive trend in Mg/Ca of well-preserved belemnites. This shift is located in sediments of the *jamesoni* and *ibex* Zs. but their biostratigraphy does not allow locating it more precisely and this trend correlate with an ambiguous positive $\delta^{13}C$ shift.

All these data indicate that the climate conditions during the negative Sinemurian-Pliensbachian boundary event are still not well constrained and difficult to correlate with the Breggia section. A different climatic pattern between the European sections may be explained by the presence of more humid and arid climate belts (Boucot and Scotese, 2013), by a widespread hiatus or by a diagenetic overprint in some of the studied sections. Furthermore, it should not be forgotten that humid climates do not necessarily imply warming and vice versa. Hydrological conditions and temperature changes should be considered separately and thus render the climatic interpretations even more difficult. In the UK and northern France, a major hiatus exactly at the Sinemurian-Pliensbachian boundary obliterated an important part of the negative Sinemurian-Pliensbachian boundary CIE (Hesselbo and Jenkyns, 1998; Bougeault et al., 2017). Therefore, is it not excluded that at the beginning of the negative CIE a warming and/or more humid phase occurred in these areas, which was not recorded or preserved. This would imply that there only the onset of the negative CIE is characterised by warmer and/or more humid conditions in contrary to the remainder of this long CIE, during which drier and/or cooler conditions were recorded.

The concomitant negative CIE is generally interpreted as the result of increased input of light carbon due to a late phase in CAMP volcanic activity (e.g., Rühl et al., 2016), and/or to increased rifting associated with volcanic activity related to the opening of the Hispanic Corridor (Porter et al., 2013; Franceschi et al., 2014). Independently, both mechanisms imply an increase in atmospheric pCO_2 inducing global warming. Alternatively, Danisch et al. (2019) explained this CIE by the return to background values following a positive late Sinemurian CIE. However, given the very low $\delta^{13}C$ values reached during the Sinemurian- Pliensbachian CIE, which represent the lightest values measured not only in the entire section of the Breggia, but also in most other sections (Fig. 8), an interpretation of reinforced input of light carbon into the exogenic reservoirs as a driver of this important negative CIE is more likely (Schöllhorn et al., 2020).

5.4.5.2. The negative CIEs in the davoei and margaritatus Zones. Correlations between the two small negative CIEs associated with increased P

Table 2
Compilation of the localities, carbon carrier, amplitudes and references from the studies recording carbon isotopic events during the Pliensbachian.

$\delta^{13}C$ events	C carrier	Locality	$\delta^{13}C$ CIE amplitude	References
Sinemurian-Pliensbachian boundary N CIE	Bulk OM	UK	3–4‰	Schöllhorn et al., 2020; van de Schootbrugge et al., 2005
		France	2–4‰	Peti et al., 2017; Mercuzot et al., 2020
		Morocco	3‰	Mercuzot et al., 2020
		Canada		Caruthers et al., 2014
	OM HI-corrected	UK	2‰	Schöllhorn et al., 2020
	Wood	UK	4‰	Korte and Hesselbo, 2011
		Portugal		Suan et al., 2010
	Bulk carbonate	UK	2‰	van de Schootbrugge et al., 2005
		Morocco	2‰	Mercuzot et al., 2020
		France	1–1.5‰	Bougeault et al., 2017; Mercuzot et al., 2020
		Portugal	2–3‰	Oliveira et al., 2006; Duarte et al., 2014
		Italy	1.5–3‰	Morettini et al., 2002; Speranza and Parisi, 2007; Woodfine et al., 2008; Marino and Santantonio, 2010; Franceschi et al., 2014
		Switzerland		This study
	Belemnites	UK	3‰	Korte and Hesselbo, 2011; Price et al., 2016
		Spain	1–3‰	Rosales et al., 2006; Armendáriz et al., 2012; Gómez et al., 2016
	Other calcitic organisms	UK	4‰	Korte and Hesselbo, 2011
		Algeria	6‰	Baghli et al., 2020
		Portugal	2.5‰	Suan et al., 2010, Ferreira et al., 2019
Upper Pliensbachian P CIE	Bulk OM	UK	3.5–6‰	Van de Schootbrugge et al., 2005; Schöllhorn et al., 2020
		Morocco	4‰	Mercuzot et al., 2020
		France	5‰	Peti et al., 2017; Mercuzot et al., 2020
		Canada and USA	3‰	Caruthers et al., 2014
	OM HI corrected	UK	3.5‰	Schöllhorn et al., 2020
	Wood	UK	8‰	Korte and Hesselbo, 2011
		Portugal	3‰	Suan et al., 2010
	Bulk carbonate	UK	2.5–4‰	Van de Schootbrugge et al., 2005
		Portugal	2‰	Oliveira et al., 2006; Silva et al., 2011
		Morocco	3‰	Mercuzot et al., 2020
		France	2‰	Van de Schootbrugge et al., 2010; Harazim et al., 2013
		Italy	1.5‰	Morettini et al., 2002; Speranza and Parisi, 2007; Woodfine et al., 2008; Marino and Santantonio, 2010
		Switzerland	>1.5‰	Jenkyns and Clayton, 1986; This study
	Belemnites	UK	4‰	Bailey et al., 2003; Korte and Hesselbo, 2011; Price et al., 2016
		Spain	2.5–3.5‰	Rosales et al., 2004a, 2004b; Gómez et al., 2016
	Other calcitic organisms	UK	4‰	Korte and Hesselbo, 2011
		Algeria	3‰	Baghli et al., 2020
		Portugal	3‰	Suan et al., 2010
Davoei N CIE	Bulk OM	Canada	1‰	Caruthers et al., 2014
		UK	1‰	Schöllhorn et al., 2020
		Morocco	1.5‰	Mercuzot et al., 2020
		France	2–3‰	Peti et al., 2017; Mercuzot et al., 2020
	OM HI corrected	UK	1‰	Schöllhorn et al., 2020
	Wood	UK	2‰	Korte and Hesselbo, 2011
	Bulk carbonate	Portugal	1–2‰	Oliveira et al., 2006; Rosales et al., 2006; Silva et al., 2011
		Morocco	1.5‰	Mercuzot et al., 2020
		France	>1‰	Bougeault et al., 2017
		Italy	>1‰	Woodfine et al., 2008; Marino and Santantonio, 2010
		UK	1‰	van de Schootbrugge et al., 2005
		Switzerland	<1‰	This study
	Belemnites	UK	2‰	Korte and Hesselbo, 2011
Margaritatus N CIE	Bulk OM	Canada	2‰	Caruthers et al., 2014
		UK	1‰	Schöllhorn et al., 2020
		Morocco	1.5‰	Mercuzot et al., 2020
		France	1.5–3‰	Peti et al., 2017; Mercuzot et al., 2020
	OM HI corrected	UK	1‰	Schöllhorn et al., 2020
	Bulk carbonate	Portugal	1‰	Oliveira et al., 2006; Silva et al., 2011
		Morocco	2‰	Mercuzot et al., 2020
		Italy		Woodfine et al., 2008
		Chile	2‰	Fantasia et al., 2018c
		Switzerland	<1‰	This study
	Belemnites	Spain	2‰	Quesada et al., 2005
Spinatum N CIE	Bulk OM	France	2–4‰	Peti et al., 2017; Mercuzot et al., 2020
	Wood	UK		Korte and Hesselbo, 2011
	Bulk carbonate	France	3‰	Harazim et al., 2013
		Italy	1.5‰	Woodfine et al., 2008
		UK	1.5‰	van de Schootbrugge et al., 2005
		Portugal	2‰	Oliveira et al., 2006
		Switzerland	2‰	This study
	Belemnites	Carpathians	2‰	Arabas et al., 2017
		UK	2‰	Mc arthur et al., 2000; Bailey et al., 2003; Korte and Hesselbo, 2011
		Spain	2.5‰	Quesada et al., 2005

(continued on next page)

Table 2 (*continued*)

$\delta^{13}C$ events	C carrier	Locality	$\delta^{13}C$ CIE amplitude	References
	Other calcitic organisms	UK	3‰	Korte and Hesselbo, 2011
Pliensbachian-Toarcian boundary N CIE	Bulk OM	UK	2–3‰	Littler et al., 2010; Xu et al., 2018
		Italy	2‰	Trecalli et al., 2012
		France		Peti et al., 2017
		Luxembourg	4‰	Ruebsam et al., 2019
		Japan		Gröcke et al., 2011
		Poland	2‰	Hesselbo and Pieńkowski, 2010
	Wood	Portugal	3‰	Hesselbo et al., 2007
	Bulk carbonate	Morocco	2–5‰	Bodin et al., 2010, 2016; Ait-Itto et al., 2017
		Italy	3‰	Trecalli et al., 2012
		Portugal	2.5–4‰	Hesselbo et al., 2007
		Chile	3‰	Fantasia et al., 2018c
		Switzerland	1‰?	This study
	Belemnites	Portugal	3‰	Hesselbo et al., 2007
	Other calcitic organisms	Algeria	1‰	Baghli et al., 2020
		Portugal	2‰	Suan et al., 2008, 2010

contents in the Breggia section (Fig. 5) may be explained by hot and/or humid snaps recorded within the *davoei-margaritatus* Zs. (Silva and Duarte, 2015; Bougeault et al., 2017; Peti and Thibault, 2017; Schöllhorn et al., 2020). Negative oxygen isotope shifts may be recorded but they are not really well expressed due to the high background noise. During the *davoei*-earliest *margaritatus* interval, Silva and Duarte (2015) identified two warm peaks, which coincide with regional deposition of organic matter-rich sediments in Spain and Portugal (Silva and Duarte, 2015), and a decline in the diversity of ammonite species (Dommergues et al., 2009). Increased runoff and/or higher temperatures are indicated by clay minerals (Paris Basin, Wessex Basin, Cardigan Bay Basin, European compilation between 30 and 40°N) (Dera et al., 2009a; Bougeault et al., 2017; Deconinck et al., 2019; Schöllhorn et al., 2020), an increase in the chemical alteration index (Wessex Basin) (Schöllhorn et al., 2020) and a decrease in $\delta^{18}O$ values (Wessex Basin: Price et al., 2016; Schöllhorn et al., 2020; Cleveland Basin: Korte and Hesselbo, 2011; and in a European compilation of $\delta^{18}O$ data in fish teeth: Dera et al., 2009b). This interval coincides with a positive εNd excursion implying that the incursion of warm-water masses from the equatorial Tethys was a main factor conditioning climate belts during at least the *davoei* Z. (Dera et al., 2009b, 2014).

In the *margaritatus* Z., three short-lived warming events were recognised in the Lusitanian basin (Silva and Duarte, 2015) based on oxygen isotopes (Oliveira et al., 2009; Suan et al., 2010). They correlate with organic matter-enriched deposits, minor ammonite extinctions in the Mediterranean realm, selective bivalve extinctions (Aberhan and Baumiller, 2003) and the small size of *Schizophaerella* during warming (Suan et al., 2010; Peti and Thibault, 2017). In addition, climate fluctuations were also observed in the Wessex Basin (clay minerals and chemical index of alteration) (Schöllhorn et al., 2020) and in the Paris Basin (Bougeault et al., 2017) and may therefore support the evidence for these climate snaps. However, correlation of these events through different localities remains difficult.

5.4.5.3. Long-term trend during the upper margaritatus-spinatum Zones. In the Breggia section, the most positive values in the $\delta^{18}O$ data, which may indicate a cooler temperature, were recorded in sediments corresponding to the top of the *margaritatus* Z. and the *spinatum* Z. Low P contents were recorded during this interval concomitant with low continental runoff. In addition, an increase in the illite content at the expense of smectite is recorded in the upper Pliensbachian, which may indicate a shift towards drier conditions (Fig. 5).

Several studies have suggested that the late Pliensbachian is characterised by cooler seawater and atmospheric temperatures. This is evidenced by oxygen isotope data and Mg/Ca ratios in sections in Algeria (Baghli et al., 2020), Portugal (Oliveira et al., 2006; Suan et al., 2008, 2010), Spain (Rosales et al., 2004a, 2004b, 2006, 2018; Quesada et al., 2005; van de Schootbrugge et al., 2005; Gómez et al., 2016; Val et al., 2017), United Kingdom (Bailey et al., 2003; Korte and Hesselbo,

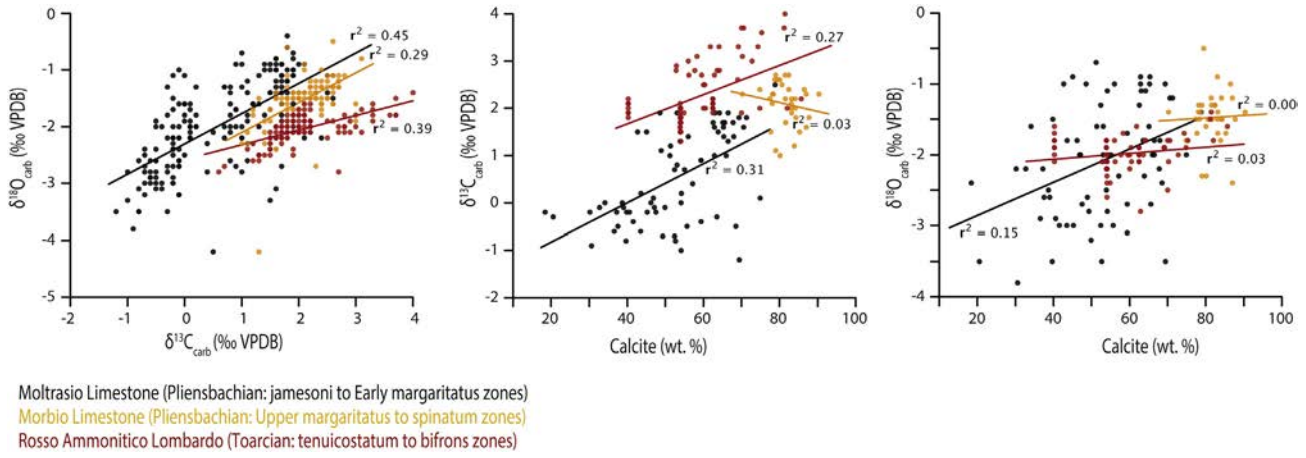


Fig. 9. Cross-plots between oxygen and carbon isotope data performed on bulk carbonate ($\delta^{18}O_{carb}$ and $\delta^{13}C_{carb}$) and calcite content in order to evaluate the influence of diagenesis along the Breggia section.

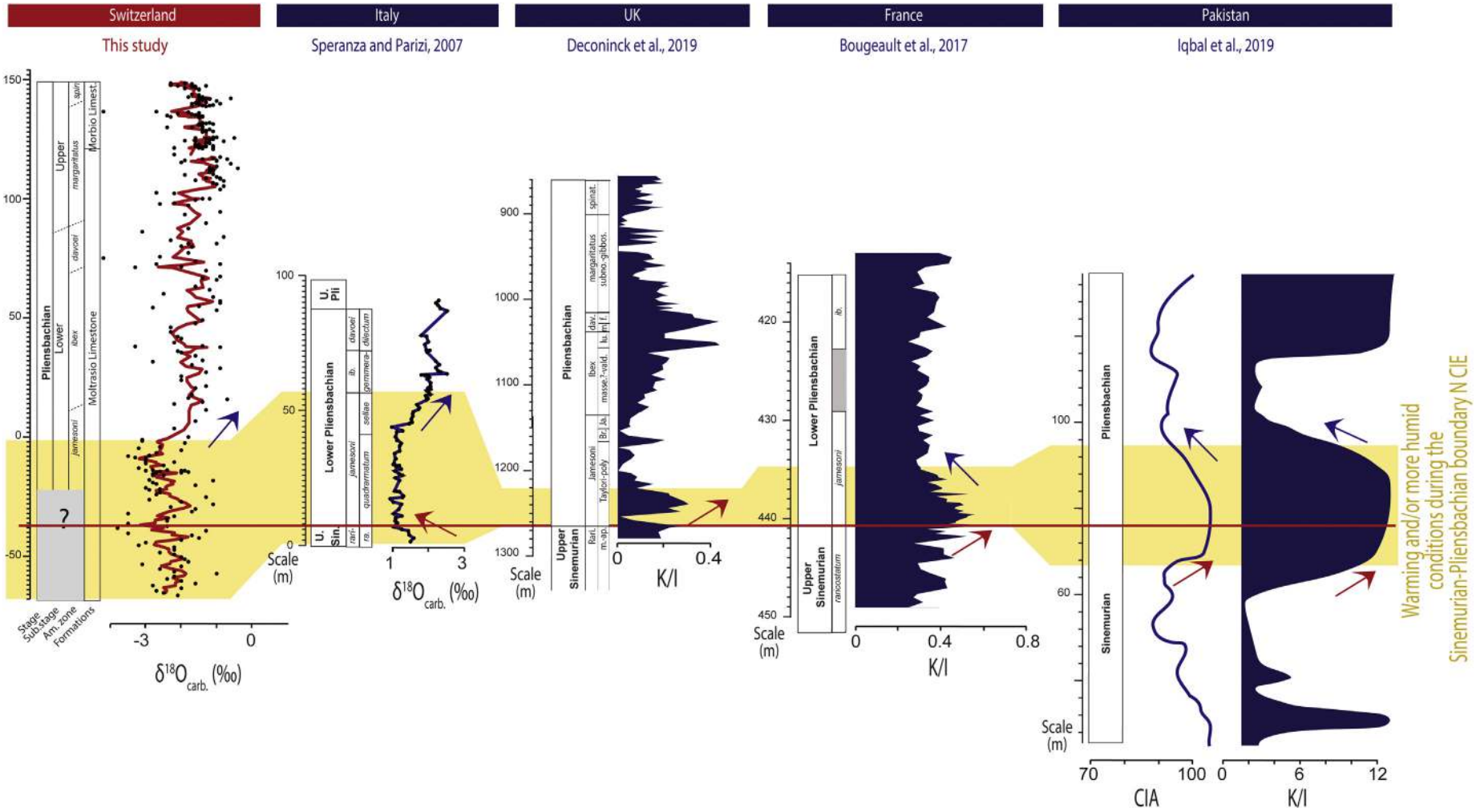


Fig. 10. Compilation of evidence for warming and/or more humid conditions during the Sinemurian-Pliensbachian boundary negative CIE (oxygen isotope data obtained from bulk carbonate: $\delta^{18}O_{carb}$; kaolinite/illite ratio: K/I; chemical alteration index: CIA) (Nesbitt and Young, 1982, 1989).

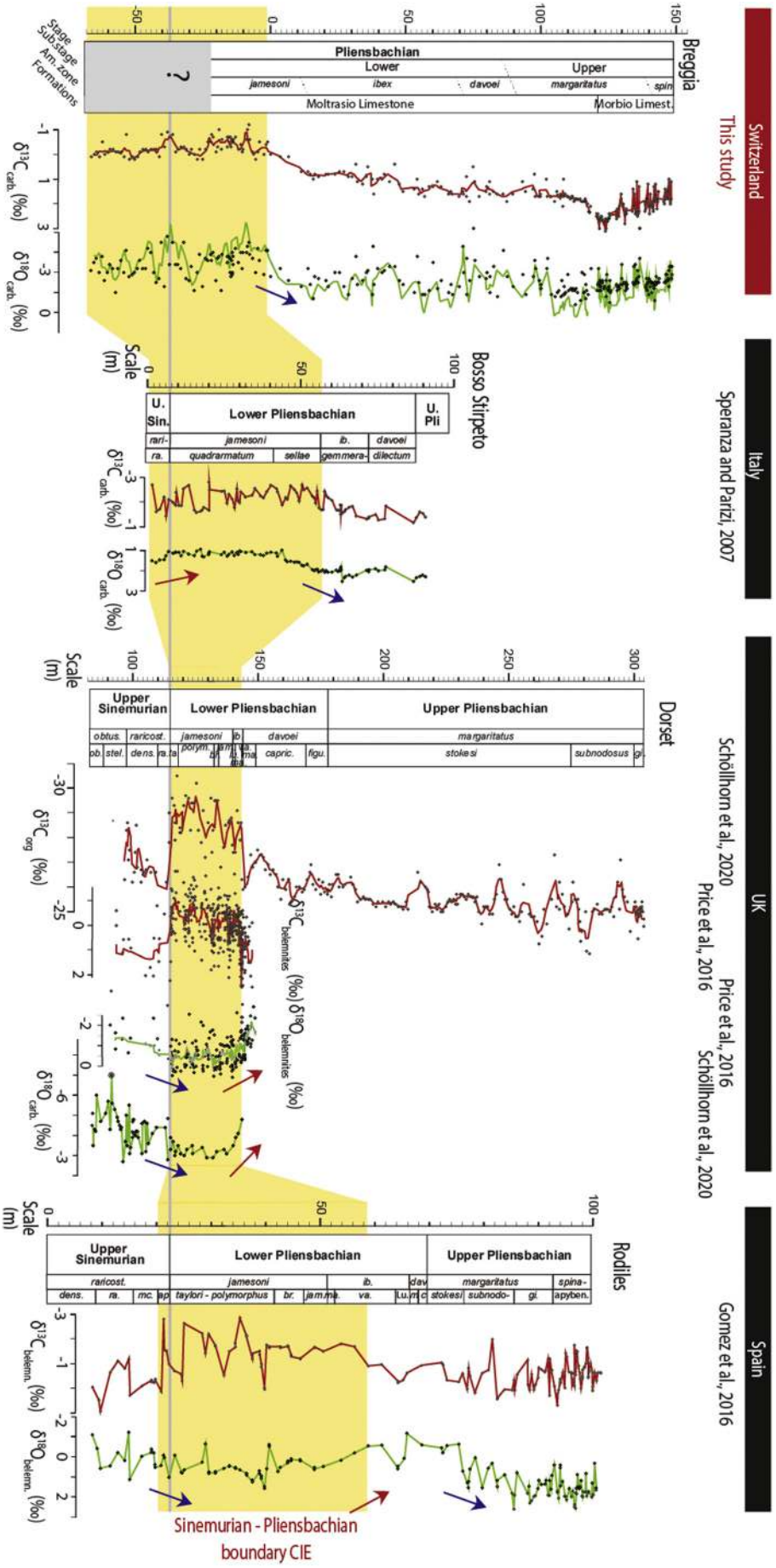


Fig. 11. Compilation of carbon and oxygen isotope records ($\delta^{13}C$ and $\delta^{18}O$) for the Sinemurian-Pliensbachian boundary negative CIE.

2011), the Carpathians (Arabas et al., 2017), and France (Harazim et al., 2013). Lower runoff is also suggested by a sharp decrease in the kaolinite/illite ratio reported in a European compilation by Dera et al. (2009b) and in France (Bougeault et al., 2017; Peti et al., 2017). The distribution of *Xenoxylon* (gymnosperm-like wood) and palynological studies from western Europe and China are also in support of a general cooling during this period (Philippe and Thevenard, 1996; Wang et al., 2005).

The occurrence of glendonite, tillite, and dropstones in polar regions (Kaplan, 1978; Price, 1999; Rogov and Zakharov, 2010; Teichert and Luppold, 2013; Philippe et al., 2017) sustains the hypothesis of the presence of ice sheets in line with sea level regression and general cooling (Hallam, 1998; Price, 1999; Suan et al., 2008, 2010; Steinthorsdottir and Vajda, 2013; Haq, 2017; Ruebsam et al., 2019). Nevertheless, this glacioeustatic interpretation remains questionable, as the sedimentological evidence for glaciation is altogether sparse.

In the Breggia section, cooler and drier conditions are associated with the positive $\delta^{13}C$ CIE recorded in the upper Pliensbachian (culminating in the *margaritatus* Z.) and continues during the following negative CIE recorded in the *spinatum* Z. This pattern is also recorded in isotope data from sections in France, Portugal, Carpathians, and Germany (Bailey et al., 2003; Oliveira et al., 2006; Suan et al., 2008, 2010; Harazim et al., 2013; Arabas et al., 2017).

Enhanced preservation of organic matter may have led to increased carbon storage and decreased atmospheric pCO_2 during the latest *margaritatus–spinatum* Zs. (late Pliensbachian; Berner, 1994; Berner and Kothavala, 2001; Bergman et al., 2004; Royer, 2006; Price et al., 2013; Steinthorsdottir and Vajda, 2013) and may therefore have triggered or amplified this cooling event (Suan et al., 2010; Korte and Hesselbo, 2011; Silva et al., 2011). In addition, lower CO_2 input due to lower volcanic activity an/or changes in current pattern during the break-up of Pangaea might have contributed to climate change (Schöllhorn et al., 2020).

5.4.5.4. The negative CIE at the Pliensbachian/Toarcian boundary. At Breggia, the possible negative shift in the $\delta^{13}C$ data seems to coincide with a decrease in $\delta^{18}O$ data and a slightly increased P content, suggesting a warmer more humid climate with increased runoff during the Pliensbachian-Toarcian boundary interval.

An enhanced hydrological cycle and possible higher temperatures on the continent, resulting in enhanced nutrient delivery into the sea are also shown by oxygen isotope and Mg/Ca data in sections in Spain and Portugal (Rosales et al., 2004a, 2004b; Suan et al., 2008), increased P content in a section in Morocco (Bodin et al., 2010), increased kaolinite content in a section in Chile (Fantasia et al., 2018c), an increase in the $^{187}Os/^{188}Os$ ratio (Percival et al., 2016) and by ammonite migrations (Mouterde and Ruget, 1975; Macchioni and Cecca, 2002).

5.4.6. Comparison with the T-OAE

At Breggia, the negative CIE recorded during the T-OAE coincides with a decrease in the $\delta^{18}O$ ratios and a slight increase in P content (Fantasia et al., 2018a, 2018b), which is very similar to the trends observed in the precedent negative CIEs (Fig. 5). Even if the magnitude of the CIE and climate impact were different, the comparable trends indicate that the climate response was similar for all these negative CIEs implying comparable mechanisms.

In our study, the increase in P coeval with the decrease in $\delta^{18}O$ ratio was interpreted as an indicator of higher temperatures and increased runoff (Fig. 5). The absence of a coeval increase in kaolinite (Fantasia et al., 2018b) may be explained by the deeper and more distal setting during this time interval at the Breggia site (Cobianchi and Picotti, 2001) and/or by a climate that may have been not sufficiently hydrolysing to create kaolinite in important amounts (Fantasia et al., 2018b). Already the upper Pliensbachian sediments are characterised by low kaolinite content suggesting that the clay composition was related to a long-term phenomenon not only characterising the lowermost Toarcian T-OAE (Fig. 5) (Dera et al., 2009b; Hermoso and Pellenard, 2014; this study). The increase in kaolinite observed from the upper *falciferum* Z. onward (Toarcian) (Deconinck and Bernoulli, 1991; Fantasia et al., 2018b) may be related to a return to a depositional setting favourable to the deposition of kaolinite (sea-level fall) (Cobianchi and Picotti, 2001) and possibly a coeval strong terrigenous input (Deconinck and Bernoulli, 1991).

5.5. Causes of these events

5.5.1. Mercury content in the Breggia and Dorset sections

5.5.1.1. Breggia section. In the Breggia section, the Hg spikes are 2–3 orders of magnitude higher than the average background values (Fig. 5). They correlate with higher P content and negative shifts in $\delta^{13}C_{carb}$ and for the lowermost Pliensbachian with $\delta^{18}O_{carb}$ data (Fig. 5).

In the Breggia section the Hg content is quite low on average (0.2 to 34 ppb), likely because of the distal setting. Normalisation by TOC is not possible as the average content is below 0.2 wt%. The few samples containing more TOC (up to 0.42 wt%) are recorded between −55 and −25 m coinciding with the negative CIE near the Sinemurian-Pliensbachian boundary which include several Hg spikes (Figs. 5, 12). However, as the Hg spikes within the negative CIEs near the Sinemurian-Pliensbachian boundary and in the *davoei*

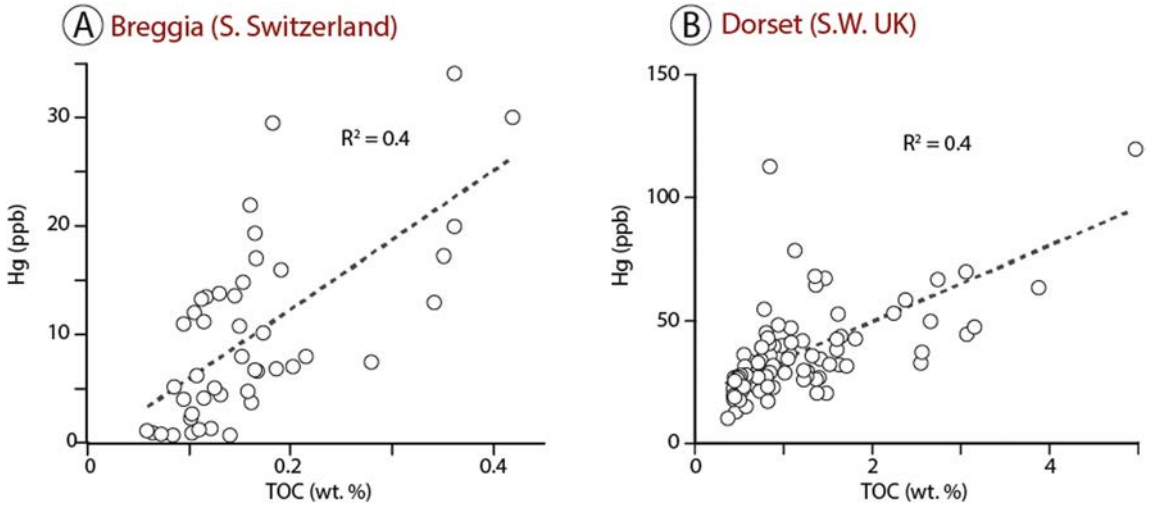


Fig. 12. Cross plots between Hg content, phyllosilicate, and organic carbon (TOC) contents from the Breggia (A) and Dorset (b) sections.

and *margaritatus* Zs. do not coincide with high TOC contents, they may not be driven by organic matter scavenging. Also, the correlation between phyllosilicate and Hg contents is rather low (R^2 = 0.03) and therefore the positive anomalies in Hg content do not appear to be primarily controlled by clay content variations. However, within the *davoei* and *margaritatus* Zs. some Hg spikes coincide with higher phyllosilicate contents of and thus may be partly explained by adsorption onto clay.

A reduction in sedimentation rate may result in increased bulk-rock Hg content. However, the Moltrasio Formation is characterised by high sedimentation rates in a rapidly subsiding basin, which received high amounts of sediments (Stockar, 2003). The analysed samples are not characterised by reduced sedimentation rates and hardgrounds. Therefore, this mechanism is unlikely to be driving the occurrence of Hg spikes. Warmer and more humid climate conditions reflected by P content and oxygen isotopes, coincide with the observed Hg spikes.

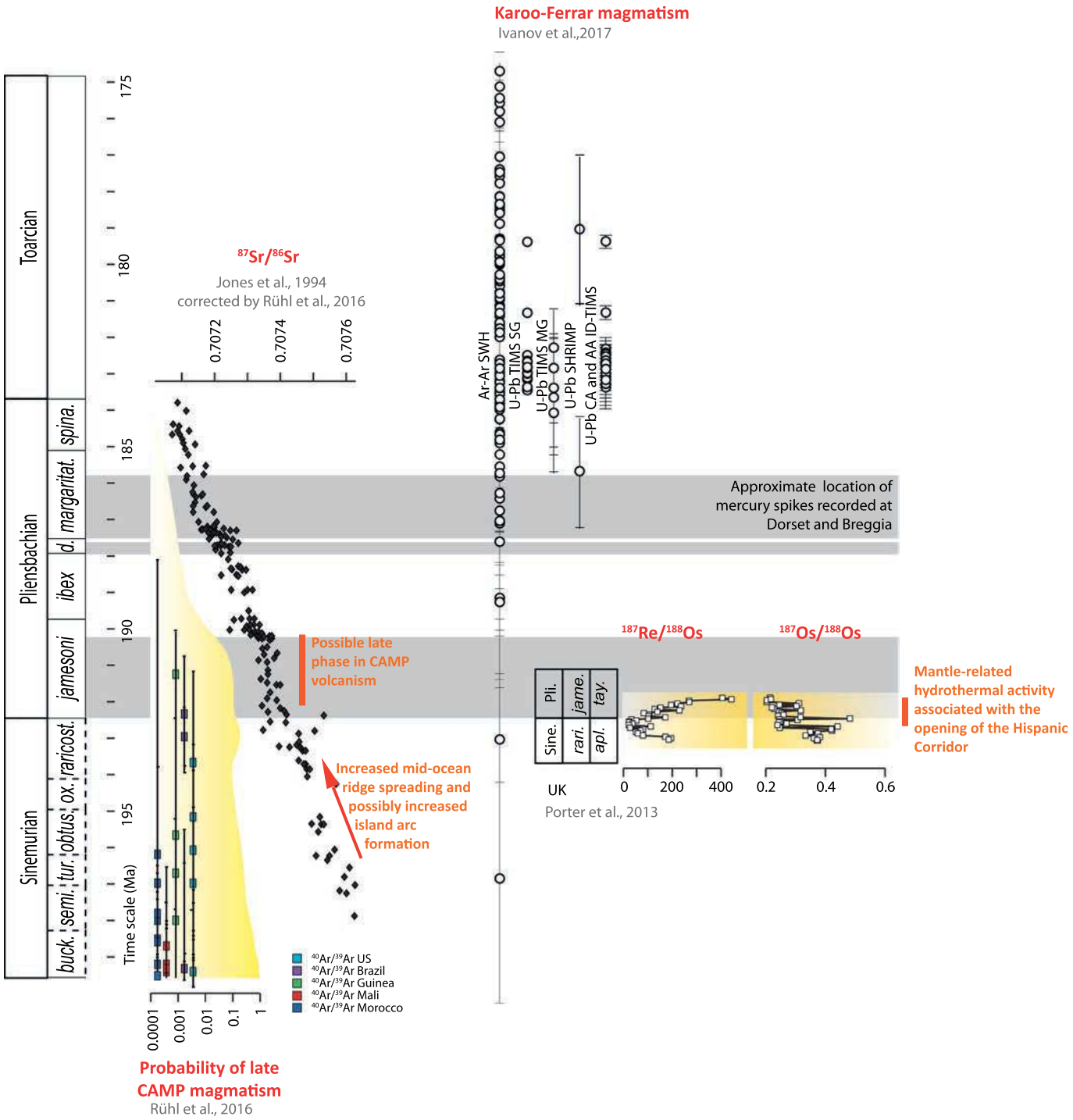


Fig. 13. Ages for CAMP and Karoo Ferrar volcanism during the Sinemurian-Pliensbachian interval compared to strontium isotopes ($^{87}Sr/^{86}Sr$) and osmium and rhenium isotopes ($^{187}Re/^{188}Os$; $^{187}Os/^{188}Os$). The CAMP ages are recalculated by Rühl et al. (2016) based on data from Baksi and Archibald (1997); Deckart et al. (1997); Marzoli et al. (1999, 2004, 2011); Hames et al. (2000); Knight et al. (2004); Beutel et al. (2005); Verati et al. (2007); Nomade et al. (2007) and Jourdan et al. (2009). The Karoo-Ferrar ages are recalculated by Ivanov et al. (2017) based on data from Landoll et al. (1989); Foland et al. (1993); Heimann et al. (1994); Brewer et al. (1996); Encarnación et al. (1996); Duncan et al. (1997); Williams and Hergt (2000); Jones and Jenkyns (2001); Le Gall et al. (2002); Zhang et al. (2003); Jourdan et al. (2004, 2005, 2007); Riley et al. (2004, 2006); Svensen et al. (2012); White and Ireland (2012); Sell et al. (2014); Burgess et al. (2015) and Ivanov et al. (2017).

In the sediments of the Morbio Limestone, no Hg enrichments are recorded and average values are very low (around 1 ppb). In this unit, the depositional area may have become too distal to record any Hg enrichment.

5.5.1.2. Dorset section. Along the Dorset coast, the Hg content ranges from 4 to 120 ppb with three intervals recording substantially higher values (Fig. 7). They correspond, as for the Breggia section, to the *jamesoni* Z. (up to 120 ppb), the lower *davoei* Z. (up to 78 ppb), and the lower *margaritatus* Z. (up to 112 ppb). In this section, the samples are characterised by an average TOC content of 1.1 wt%, with outliers going from 0.4 up to 5 wt%. On the Hg vs. TOC plot the correlation is low ($R^2 = 0.4$), but a generally positive trend is observed (Fig. 12B). This may reflect the possibility that organic matter is the main Hg contributor and thus the Hg content was normalised by the corresponding TOC content (Sanei et al., 2012; Percival et al., 2015; Thibodeau et al., 2016; Grasby et al., 2017; Fantasia et al., 2018b). After normalising, several spikes remained, suggesting that they are possibly not linked to organic matter scavenging (Fig. 7). The Hg spikes, recorded in the *davoei* and *margaritatus* Zs., coincide with more humid and warmer conditions, as suggested by the chemical alteration index and kaolinite content (Schöllhorn et al., 2020).

5.5.2. Implications

The Hg data provided from the Breggia and Dorset sections highlight the existence of possibly correlative peaks coinciding with the Sinemurian-Pliensbachian negative CIE and during the *davoei* and *margaritatus* Zs., which partly persist following TOC normalisation. One recent study (Lena et al., 2019) records a Hg spike in Northern America within the *margaritatus* Z. which could correlate with the Hg spike observed in the Dorset and Breggia sections. However, to date we are not aware of any other report covering the entire Pliensbachian. Therefore, it remains difficult to evaluate the spatial persistence of the Hg enrichments beyond these three sections. This would be necessary in order to interpret the Hg record as possibly influenced by changes in volcanic activity.

In the case of a volcanogenic origin, the Hg spikes recorded within the earliest Pliensbachian may coincide with a late phase of the CAMP and/or increased rifting during the opening of the Hispanic corridor. Rühl et al. (2016) compiled $^{40}Ar/^{39}Ar$ records suggesting that a late phase of CAMP activity coincided with the earliest Pliensbachian (*jamesoni* Z.) negative CIE (Fig. 13). Furthermore, this observation is supported by $^{87}Sr/^{86}Sr$ data from Jones et al. (1994), Jenkyns et al. (2002) and Rühl et al. (2016) (Fig. 13). The opening of the Hispanic Corridor connecting the eastern Pacific and Tethys around the Sinemurian-Pliensbachian boundary is evidenced by biogeographic and faunal exchange patterns (Damborenea and Manceñido, 1979; Hallam, 1983; Smith, 1983; Smith and Tipper, 1986; Smith et al., 1990; Aberhan, 2001; Arias, 2006, 2007; Venturi et al., 2006, 2007), and $^{187}Os/^{186}Os$ isotopes (Porter et al., 2013) (Fig. 13).

The Hg spikes from the *davoei* and *margaritatus* Zs. may correspond to an early phase in Karoo-Ferrar volcanic activity or also to rifting phases. Indeed, a Pliensbachian $^{40}Ar/^{39}Ar$ age was highlighted for the beginning of the Karoo-Ferrar large igneous province (LIP) (Fig. 13) (182 to 172 Myr; 188 to 153 Myr; Pankhurst et al., 2000; 186 to 176 Myr; Jourdan et al., 2008).

However, all the Pliensbachian ages (*jamesoni* to the *margaritatus* Zones) for the CAMP and Karoo-Ferrar volcanism were measured (Fig. 13) several years ago and thus include large incertitudes due to measurement and calculation approximation. Therefore, until now a late phase of CAMP volcanism or early phases of the Karoo-Ferrar remain speculative. If these Hg spikes are not confirmed in other basins, then they are likely to be related to local conditions like increased terrestrial inputs or differential scavenging in organic matter and clays.

6. Conclusions

A set of geochemical analyses was performed on Pliensbachian hemipelagic sediments in the Breggia Gorge (southern Switzerland) close to the open Tethys (Schöllhorn, 2019). Negative carbon isotope excursions are recorded near the Sinemurian/Pliensbachian boundary, in the *davoei*, *margaritatus*, and *spinatum* Zs., and possibly near the Pliensbachian-Toarcian boundary. These events coincide with environmental conditions characterised by higher temperatures and increased runoff bringing in more nutrients, based on coeval increases in whole-rock oxygen isotope data and phosphorus content. This pattern is also observed during the T-OAE in the same section (Fantasia et al., 2018a, 2018b) suggesting climate and environmental responses similar for all CIE's.

In addition, Hg analyses were performed for the first time on the entire Pliensbachian. The record from the Breggia section was compared to a section near Lyme Regis and Charmouth along the Dorset coast (southern England). The occurrence of Hg spikes in both sections during the Sinemurian-Pliensbachian boundary event and within the *davoei* and *margaritatus* Zs. may go in line with volcanic events. The Hg spikes recorded within the earliest Pliensbachian may coincide with a late phase of the CAMP and/or increased rifting during the opening of the Hispanic Corridor. Otherwise, the Hg spikes from the *davoei* and *margaritatus* Zs. may correspond to an early phase in Karoo-Ferrar volcanic activity or increased rifting. Further analyses are, however, needed to investigate the importance of increased terrestrial input and differential scavenging on organic matter and clays and ascertain the role of increased volcanic activity in Hg enrichment.

Declaration of competing interest

The authors declare the following financial interests/personal relationships which may be considered: as potential competing interests: this paper is part of a PhD thesis deposited in the Library of the University of Lausanne.

Acknowledgements

We would like to acknowledge the logistical and financial support of the University of Lausanne which financed the PhD thesis at the origin of this paper (Schöllhorn, 2019). We thank both Tiffany Monnier and Jean-Claude Lavanchy for their assistance in the laboratories, Alicia Fantasia and Yoann Chevalier for their help in the field. We thank the Cantonal Natural Museum of Lugano, Rudolf Stockar and Marco Antognini for the sampling permission in the Breggia gorges. Furthermore, we would like to acknowledge the reviewers Nicolas Thibault and Pierre Pellenard for their constructive advice that improved this study considerably.

References

Aberhan, M., 2001. Bivalve palaeobiogeography and the Hispanic Corridor: time of opening and effectiveness of a proto-Atlantic seaway. Palaeogeogr. Palaeoclimatol. Palaeoecol. 165, 375–394.

Aberhan, M., Baumiller, T.K., 2003. Selective extinction among Early Jurassic bivalves: a consequence of anoxia. Geology 31, 1077–1080.

Adatte, T., Stinnesbeck, W., Keller, G., 1996. Lithostratigraphic and mineralogic correlations of near K/T boundary clastic sediments in northeastern Mexico: implications for origin and nature of deposition. Geol. Soc. Am. Spec. Pap. 307, 211–226.

Ait-Itto, F.-Z., Price, G.D., Addi, A.A., Chafiki, D., Mannani, I., 2017. Bulk-carbonate and belemnite carbon-isotope records across the Pliensbachian-Toarcian boundary on the northern margin of Gondwana (Issouka, Middle Atlas, Morocco). Palaeogeogr. Palaeoclimatol. Palaeoecol. 466, 128–136.

Arabas, A., Schlögl, J., Meister, C., 2017. Early Jurassic carbon and oxygen isotope records and seawater temperature variations: Insights from marine carbonate and belemnite rostra (Pieniny Klippen Belt, Carpathians). Palaeogeogr. Palaeoclimatol. Palaeoecol. 485, 119–135.

Arias, C., 2006. Northern and Southern Hemispheres ostracod palaeobiogeography during the Early Jurassic: possible migration routes. Palaeogeogr. Palaeoclimatol. Palaeoecol. 233, 63–95.

Arias, C., 2007. Pliensbachian–Toarcian ostracod biogeography in NW Europe: evidence for water mass structure evolution. Palaeogeogr. Palaeoclimatol. Palaeoecol. 251, 398–421.

Armendáriz, M., Rosales, I., Bádenas, B., Aurell, M., García-Ramos, J.C., Piñuela, L., 2012. High-resolution chemostratigraphic records from Lower Pliensbachian belemnites: Palaeoclimatic perturbations, organic facies and water mass exchange (Asturian basin, northern Spain). Palaeogeogr. Palaeoclimatol. Palaeoecol. 333–334, 178–191.
Baghli, H., Mattioli, E., Spangenberg, J.E., Bensalah, M., Arnaud-Godet, F., Pittet, B., Suan, G., 2020. Early Jurassic climatic trends in the south-Tethyan margin. Gondwana Res. 77, 67–81.
Bailey, T.R., Rosenthal, Y., McArthur, J.M., van de Schootbrugge, B., Thirlwall, M.F., 2003. Paleoceanographic changes of the Late Pliensbachian–early Toarcian interval: a possible link to the genesis of an Oceanic Anoxic Event. Earth Planet. Sci. Lett. 212, 307–320.
Baksi, A.K., Archibald, D., 1997. Mesozoic igneous activity in the Maranhano province, northern Brazil: 40Ar/39Ar evidence for separate episodes of basaltic magmatism. Earth Planet. Sci. Lett. 151, 139–153.
Behar, F., Beaumont, V., Penteado, H.D.B., 2001. Rock-Eval 6 technology: performances and developments. Oil Gas Sci. Technol. 56, 111–134.
Benoit, J., Mason, R.P., Gilmour, C.C., Aiken, G.R., 2001. Constants for mercury binding by dissolved organic matter isolates from the Florida Everglades. Geochim. Cosmochim. Acta 65, 4445–4451.
Bergman, N.M., Lenton, T.M., Watson, A.J., 2004. COPSE: a new model of biogeochemical cycling over Phanerozoic time. Am. J. Sci. 304, 397–437.
Berner, R., 1994. Geocarb, II: a revised model of atmospheric CO2 over Phanerozoic time. Am. J. Sci. 294, 56–91.
Berner, R.A., Kothavala, Z., 2001. GEOCARB III: a revised model of atmospheric CO2 over Phanerozoic time. Am. J. Sci. 301, 182–204.
Bernoulli, D., 1990. Mendrisio-Breggia Valley-Chiasso. Geology of Switzerland, a Guide-Book. Basel, Wepf.
Bertotti, G., Picotti, V., Bernoulli, D., Castellarin, A., 1993. From rifting to drifting: tectonic evolution of the South-Alpine upper crust from the Triassic to the Early Cretaceous. Sediment. Geol. 86, 53–76.
Beutel, E., Nomade, S., Fronabarger, A., Renne, P., 2005. Pangea's complex breakup: a new rapidly changing stress field model. Earth Planet. Sci. Lett. 236, 471–485.
Bjerrum, C.J., Surlyk, F., Callomon, J.H., Slingerland, R.L., 2001. Numerical paleoceanographic study of the Early Jurassic transcontinental Laurasian Seaway. Paleoceanography 16, 390–404.
Bodin, S., Mattioli, E., Fröhlich, S., Marshall, J., Boutib, L., Lahsini, S., Redfern, J., 2010. Toarcian carbon isotope shifts and nutrient changes from the northern margin of Gondwana (High Atlas, Morocco, Jurassic): palaeoenvironmental implications. Palaeogeogr. Palaeoclimatol. Palaeoecol. 297, 377–390.
Bodin, S., Krencker, F.-N., Kothe, T., Hoffmann, R., Mattioli, E., Heimhofer, U., Kabiri, L., 2016. Perturbation of the carbon cycle during the late Pliensbachian–early Toarcian: new insight from high-resolution carbon isotope records in Morocco. J. Afr. Earth Sci. 116, 89–104.
Boucot, A.J., Xu, C., Scotese, C.R., 2013. Phanerozoic paleoclimate: an atlas of lithologic indicators of climate No. 11: Map Folio. In: Nichols, G.J., Ricketts, B. (Eds.), Concepts in Sedimentology and Paleontology, Society for Sedimentary Geology Concepts, Tulsa, Oklahoma, U.S.a (30 pp).
Bougeault, C., Pellenard, P., Deconinck, J.-F., Hesselbo, S.P., Dommergues, J.-L., Bruneau, L., Cocquerez, T., Laffont, R., Huret, E., Thibault, N., 2017. Climatic and palaeoceanographic changes during the Pliensbachian (Early Jurassic) inferred from clay mineralogy and stable isotope (C-O) geochemistry (NW Europe). Glob. Planet. Chang. 149, 139–152.
Bown, P., Young, J., 1998. Calcareous Nannofossil Biostratigraphy. British Micropalaeontological Society Publication London, Springer 15 pp.
Brewer, T., Rex, D., Guise, P., Hawkesworth, C., 1996. Geochronology of Mesozoic tholeiitic magmatism in Antarctica: implications for the development of the failed Weddell Sea rift system. Geol. Soc. Lond., Spec. Publ. 108, 45–61.
Burgess, S.D., Bowring, S.A., Fleming, T.H., Elliot, D.H., 2015. High-precision geochronology links the Ferrar large igneous province with Early Jurassic ocean anoxia and biotic crisis. Earth Planet. Sci. Lett. 415, 90–99.
Caruthers, A.H., Smith, P.L., Grocke, D.R., 2014. The Pliensbachian-Toarcian (Early Jurassic) extinction: a North American perspective. Geol. Soc. Am. Spec. Pap. 505, 225–243.
Casellato, C.E., Erba, E., 2015. Calcareous nannofossil biostratigraphy and paleoceanography of the Toarcian anoxic event at Colle di Sogno (Southern Alps, Northern Italy). Riv. Ital. Paleontol. Stratigr. 121, 297–327.
Cobianchi, M., Picotti, V., 2001. Sedimentary and biological response to sea-level and palaeoceanographic changes of a Lower–Middle Jurassic Tethyan platform margin (Southern Alps, Italy). Palaeogeogr. Palaeoclimatol. Palaeoecol. 169, 219–244.
Cohen, A.S., Coe, A.L., 2002. New geochemical evidence for the onset of volcanism in the Central Atlantic magmatic province and environmental change at the Triassic-Jurassic boundary. Geology 30, 267–270.
Cohen, A.S., Coe, A.L., Bartlett, J.M., Hawkesworth, C.J., 1999. Precise Re–Os ages of organic-rich mudrocks and the Os isotope composition of Jurassic seawater. Earth Planet. Sci. Lett. 167, 159–173.
Cohen, A.S., Coe, A.L., Harding, S.M., Schwark, L., 2004. Osmium isotope evidence for the regulation of atmospheric CO2 by continental weathering. Geology 32, 157–160.
Damborenea, S.E., Manceñido, M., 1979. On the palaeogeographical distribution of the pectinid genus Weyla (Bivalvia, Lower Jurassic). Palaeogeogr. Palaeoclimatol. Palaeoecol. 27, 85–102.
Danisch, J., Kabiri, L., Nutz, A., Bodin, S., 2019. Chemostratigraphy of Late Sinemurian–Early Pliensbachian shallow-to deep-water deposits of the Central High Atlas Basin: Paleoenvironmental implications. J. Afr. Earth Sci. 153, 239–249.
Deckart, K., Féraud, G., Bertrand, H., 1997. Age of Jurassic continental tholeiites of French Guyana, Surinam and Guinea: implications for the initial opening of the Central Atlantic Ocean. Earth Planet. Sci. Lett. 150, 205–220.
Deconinck, J.-F., Bernoulli, D., 1991. Clay mineral assemblages of Mesozoic pelagic and flysch sediments of the Lombardian Basin (Southern Alps): implications for palaeotectonics, palaeoclimate and diagenesis. Geol. Rundsch. 80, 1–17.
Deconinck, J.-F., Hesselbo, S.P., Debuisser, N., Averbuch, O., Baudin, F., Bessa, J., 2003. Environmental controls on clay mineralogy of an Early Jurassic mudrock (Blue Lias Formation, southern England). Int. J. Earth Sci. 92, 255–266.
Deconinck, J.F., Hesselbo, S.P., Pellenard, P., 2019. Climatic and sea-level control of Jurassic (Pliensbachian) clay mineral sedimentation in the Cardigan Bay Basin, Llanbedr (Mochras Farm) borehole Wales. Sedimentology 66, 2769–2783.
Dera, G., Pellenard, P., Neige, P., Deconinck, J.-F., Pucéat, E., Dommergues, J.-L.J.P., 2009a. Distribution of clay minerals in Early Jurassic Peritethyan seas: palaeoclimatic significance inferred from multiproxy comparisons. Palaeogeogr. Palaeoclimatol. Palaeoecol. 271, 39–51.
Dera, G., Pucéat, E., Pellenard, P., Neige, P., Delsate, D., Joachimski, M.M., Reisberg, L., Martinez, M., 2009b. Water mass exchange and variations in seawater temperature in the NW Tethys during the Early Jurassic: evidence from neodymium and oxygen isotopes of fish teeth and belemnites. Earth Planet. Sci. Lett. 286, 198–207.
Dera, G., Brigaud, B., Monna, F., Laffont, R., Pucéat, E., Deconinck, J.-F., Pellenard, P., Joachimski, M.M., Durlet, C., 2011. Climatic ups and downs in a disturbed Jurassic world. Geology 39, 215–218.
Dera, G., Prunier, J., Smith, P.L., Haggart, J.W., Popov, E., Guzhov, A., Rogov, M., Delsate, D., Thies, D., Cuny, G., 2014. Nd isotope constraints on ocean circulation, paleoclimate, and continental drainage during the Jurassic breakup of Pangea. Gondwana Res. 27, 1599–1615.
Dommergues, J.-L., Fara, E., Meister, C., 2009. Ammonite diversity and its palaeobiogeographical structure during the early Pliensbachian (Jurassic) in the western Tethys and adjacent areas. Palaeogeogr. Palaeoclimatol. Palaeoecol. 280, 64–77.
Duarte, L.V., Comas-Rengifo, M.J., Silva, R.L., Paredes, R., Goy, A., 2014. Carbon isotope stratigraphy and ammonite biochronostratigraphy across the Sinemurian-Pliensbachian boundary in the western Iberian margin. Bull. Geosci. 89, 719–736.
Duncan, R.A., Hooper, P., Rehacek, J., Marsh, J., Duncan, A., 1997. The timing and duration of the Karoo igneous event, southern Gondwana. J. Geophys. Res. Solid Earth 102, 18127–18138.
Eaton, A., 1995. Measuring UV-absorbing organics: a standard method. J. Am. Water Works Assoc. 87, 86–90.
Encarnación, J., Fleming, T.H., Elliot, D.H., Eales, H.V., 1996. Synchronous emplacement of Ferrar and Karoo dolerites and the early breakup of Gondwana. Geology 24, 535–538.
Espitalié, J., 1986. Use of Tmax as a maturation index for different types of organic matter. Comparison with vitrinite reflectance. In: Burrus, J. (Ed.), Thermal Modelling in Sedimentary Basins. Editions Technip, Paris, pp. 475–496.
Espitalie, J., Deroo, G., Marquis, F., 1986. La pyrolyse Rock-Eval et ses applications. Troisième partie. Rev. Inst. Francais Pétrole 41, 73–89 (in French).
Fantasia, A., Föllmi, K.B., Adatte, T., Spangenberg, J.E., Mattioli, E., Reijmer, J., 2018a. Expression of the Toarcian Oceanic Anoxic Event: new insights from a Swiss transect. Sedimentology 66, 262–284.
Fantasia, A., Föllmi, K.B., Adatte, T., Spangenberg, J.E., Montero-Serrano, J.-C., 2018b. The Early Toarcian oceanic anoxic event: Paleoenvironmental and paleoclimatic change across the Alpine Tethys (Switzerland). Glob. Planet. Chang. 162, 53–68.
Fantasia, A., Föllmi, K.B., Adatte, T., Bernárdez, E., Spangenberg, J.E., Mattioli, E., 2018c. The Toarcian Oceanic Anoxic Event in southwestern Gondwana: an example from the Andean Basin, northern Chile. J. Geol. Soc. Lond. 175, 883–902.
Ferreira, J., Mattioli, E., Sucherás-Marx, B., Giraud, F., Duarte, L.V., Pittet, B., Suan, G., Hassler, A., Spangenberg, J.E., 2019. Western Tethys Early and Middle Jurassic calcareous nannofossil biostratigraphy. Earth Sci. Rev. 102908. https://doi.org/10.1016/j.earscirev.2019.102908.
Foland, K., Fleming, T., Heimann, A., Elliot, D., 1993. Potassium-argon dating of fine-grained basalts with massive Ar loss: application of the 40Ar39Ar technique to plagioclase and glass from the Kirkpatrick Basalt, Antarctica. Chem. Geol. 107, 173–190.
Föllmi, K.B., Grimm, K.A., 1990. Doomed pioneers: gravity-flow deposition and bioturbation in marine oxygen deficient environments. Geology 18, 1069–1072.
Font, E., Adatte, T., Sial, A.N., Drude de Lacerda, L., Keller, G., Punekar, J., 2016. Mercury anomaly, Deccan volcanism, and the end-Cretaceous mass extinction. Geology 44, 171–174.
Franceschi, M., Dal Corso, J., Posenato, R., Roghi, G., Masetti, D., Jenkyns, H.C., 2014. Early Pliensbachian (Early Jurassic) C-isotope perturbation and the diffusion of the Lithiotis Fauna: Insights from the western Tethys. Palaeogeogr. Palaeoclimatol. Palaeoecol. 410, 255–263.
Gaetani, M., 1975. Jurassic stratigraphy of the Southern Alps: a review. Geol. Italy 1, 377–402.
Gehrke, G.E., Blum, J.D., Meyers, P.A., 2009. The geochemical behavior and isotopic composition of Hg in a mid-Pleistocene western Mediterranean sapropel. Geochim. Cosmochim. Acta 73, 1651–1665.
Gibbs, R.J., 1967. Quantitative X-ray diffraction analysis using clay mineral standards extracted from the samples to be analysed. Clay Miner. 7, 79–90.
Godet, A., Bodin, S., Adatte, T., Föllmi, K.B., 2008. Platform-induced clay-mineral fractionation along a northern Tethyan basin-platform transect: implications for the interpretation of Early Cretaceous climate change (Late Hauterivian-Early Aptian). Cretac. Res. 29, 830–847.
Gómez, J.J., Comas-Rengifo, M.J., Goy, A., 2016. Palaeoclimatic oscillations in the Pliensbachian (Early Jurassic) of the Asturian Basin (Northern Spain). Clim. Past 12, 1199–1214.
Grasby, S.E., Beauchamp, B., Bond, D.P.G., Wignall, P.B., Sanei, H., 2015. Mercury anomalies associated with three extinction events (Capitanian Crisis, Latest Permian Extinction and the Smithian/Spathian Extinction) in NW Pangea. Geol. Mag. 153, 285–297.

Grasby, S.E., Shen, W., Yin, R., Gleason, J.D., Blum, J.D., Lepak, R.F., Hurley, J.P., Beauchamp, B., 2017. Isotopic signatures of mercury contamination in latest Permian oceans. Geology 45, 55–58.
Gröcke, D., Hori, R., Trabucho-Alexandre, J., Kemp, D., Schwark, L., 2011. An open ocean record of the Toarcian oceanic anoxic event. Solid Earth 2, 245–257.
Hallam, A., 1983. Early and mid-Jurassic molluscan biogeography and the establishment of the central Atlantic seaway. Palaeogeogr. Palaeoclimatol. Palaeoecol. 43, 181–193.
Hallam, A., 1998. The determination of Jurassic environments using palaeoecological methods. Bull. Soc. Geol. Fr. 169, 681–687.
Hames, W., Renne, P., Ruppel, C., 2000. New evidence for geologically instantaneous emplacement of earliest Jurassic Central Atlantic magmatic province basalts on the North American margin. Geology 28, 859–862.
Haq, B.U., 2017. Jurassic sea level variations: a reappraisal. Geol. Soc. Am. Bull. Today 28, 4–10.
Harazim, D., Van De Schootbrugge, B.A.S., Sorichter, K., Fiebig, J., Weug, A., Suan, G., Oschmann, W., 2013. Spatial variability of watermass conditions within the European Epicontinental Seaway during the Early Jurassic (Pliensbachian-Toarcian). Sedimentology 60, 359–390.
Heimann, A., Fleming, T., Elliot, D., Foland, K., 1994. A short interval of Jurassic continental flood basalt volcanism in Antarctica as demonstrated by 40Ar39Ar geochronology. Earth Planet. Sci. Lett. 121, 19–41.
Hermoso, M., Pellenard, P., 2014. Continental weathering and climatic changes inferred from clay mineralogy and paired carbon isotopes across the early to middle Toarcian in the Paris Basin. Palaeogeogr. Palaeoclimatol. Palaeoecol. 399, 385–393.
Hesselbo, S.P., 2008. Sequence stratigraphy and inferred relative sea-level change from the onshore British Jurassic. Proc. Geol. Assoc. 119, 19–34.
Hesselbo, S., Jenkyns, H., 1995. A comparison of the Hettangian to Bajocian successions of Dorset and Yorkshire. In: Taylor, P.D. (Ed.), Field Geology of the British Jurassic. Geological Society, London, pp. 105–150.
Hesselbo, S.P., Jenkyns, H.C., 1998. British lower Jurassic sequence stratigraphy. SEPM Spec. Publ. 60, 561–581.
Hesselbo, S.P., Pieńkowski, G., 2010. Stepwise atmospheric carbon-isotope excursion during the Toarcian oceanic anoxic event (Early Jurassic, Polish Basin). Earth Planet. Sci. Lett. 301, 365–372.
Hesselbo, S.P., Robinson, S.A., Surlyk, F., Piasecki, S., 2002. Terrestrial and marine extinction at the Triassic-Jurassic boundary synchronized with major carbon-cycle perturbation: a link to initiation of massive volcanism? Geology 30, 251–254.
Hesselbo, S.P., Jenkyns, H.C., Duarte, L.V., Oliveira, L.C.J.E., Letters, P.S., 2007. Carbon-isotope record of the Early Jurassic (Toarcian) Oceanic Anoxic Event from fossil wood and marine carbonate (Lusitanian Basin, Portugal). Earth Planet. Sci. Lett. 253, 455–470.
Horner, F., Heller, F., 1983. Lower Jurassic magnetostratigraphy at the Breggia Gorge (Ticino, Switzerland) and Alpe Turati (Como, Italy). Geophys. J. Int. 73, 705–718.
Iqbal, S., Wagreich, M., Kuerschner, W.M., Gier, S., Bibi, M., 2019. Hot-house climate during the Triassic/Jurassic transition: the evidence of climate change from the southern hemisphere (Salt Range, Pakistan). Glob. Planet. Chang. 172, 15–32.
Ivanov, A.V., Meffre, S., Thompson, J., Corfu, F., Kamenetsky, V.S., Kamenetsky, M.B., Demonterova, E.I., 2017. Timing and genesis of the Karoo-Ferrar large igneous province: New high precision U-Pb data for Tasmania confirm short duration of the major magmatic pulse. Chem. Geol. 455, 32–43.
Jenkyns, H., 1988. The early Toarcian (Jurassic) anoxic event-stratigraphic, sedimentary, and geochemical evidence. Am. J. Sci. 288, 101–151.
Jenkyns, H.C., Clayton, C.J., 1986. Black shales and carbon isotopes in pelagic sediments from the Tethyan Lower Jurassic. Sedimentology 33, 87–106.
Jenkyns, H.C., Jones, C.E., Grocke, D.R., Hesselbo, S.P., Parkinson, D.N., 2002. Chemostratigraphy of the Jurassic System: applications, limitations and implications for palaeoceanography. J. Geol. Soc. 159, 351–378.
Jones, C.E., Jenkyns, H.C., 2001. Seawater strontium isotopes, oceanic anoxic events, and seafloor hydrothermal activity in the Jurassic and Cretaceous. Am. J. Sci. 301, 112–149.
Jones, C.E., Jenkyns, H.C., Hesselbo, S.P., 1994. Strontium isotopes in Early Jurassic seawater. Geochim. Cosmochim. Acta 58, 1285–1301.
Jourdan, F., Féraud, G., Bertrand, H., Kampunzu, A., Tshoso, G., Le Gall, B., Tiercelin, J., Capiez, P., 2004. The Karoo triple junction questioned: evidence from Jurassic and Proterozoic 40Ar/39Ar ages and geochemistry of the giant Okavango dyke swarm (Botswana). Earth Planet. Sci. Lett. 222, 989–1006.
Jourdan, F., Féraud, G., Bertrand, H., Kampunzu, A.B., Tshoso, G., Watkeys, M.K., Le Gall, B., 2005. Karoo large igneous province: Brevity, origin, and relation to mass extinction questioned by new 40Ar/39Ar age data. Geology 33, 745–748.
Jourdan, F., Féraud, G., Bertrand, H., Watkeys, M., Renne, P., 2007. Distinct brief major events in the Karoo large igneous province clarified by new 40Ar/39Ar ages on the Lesotho basalts. Lithos 98, 195–209.
Jourdan, F., Féraud, G., Bertrand, H., Watkeys, M., Renne, P., 2008. The 40Ar/39Ar ages of the sill complex of the Karoo large igneous province: implications for the Pliensbachian-Toarcian climate change. Geochem. Geophys. Geosyst. 9. https://doi.org/10.1029/2008GC001994.
Jourdan, F., Marzoli, A., Bertrand, H., Cirilli, S., Tanner, L.H., Kontak, D.J., McHone, G., Renne, P.R., Bellieni, G., 2009. 40Ar/39Ar ages of CAMP in North America: implications for the Triassic–Jurassic boundary and the 40K decay constant bias. Lithos 110, 167–180.
Kaplan, M., 1978. Calcite pseudomorphoses in Jurassic and Lower Cretaceous deposits of the northern area of eastern Siberia. J. Geol. Geophys. 12, 62–70.
Keim, L., Schlager, W., 1999. Automicrite facies on steep slopes (Triassic, Dolomites, Italy). Facies 41, 15–25.
Klug, H.P., Alexander, L.E., 1974. X-ray Diffraction Procedures: For Polycrystalline and Amorphous Materials. John Wiley and Sons, New-York 992 pp.
Knight, K.B., Nomade, S., Renne, P.R., Marzoli, A., Bertrand, H., Youbi, N., 2004. The Central Atlantic Magmatic Province at the Triassic–Jurassic boundary: paleomagnetic and 40Ar/39Ar evidence from Morocco for brief, episodic volcanism. Earth Planet. Sci. Lett. 228, 143–160.
Korte, C., Hesselbo, S.P., 2011. Shallow marine carbon and oxygen isotope and elemental records indicate icehouse-greenhouse cycles during the Early Jurassic. Paleoceanography 26. https://doi.org/10.1029/2011PA002160.
Krencker, F.N., Lindström, S., Bodin, S., 2019. A major sea-level drop briefly precedes the Toarcian oceanic anoxic event: implication for Early Jurassic climate and carbon cycle. Sci. Rep. 9, 1–12. https://doi.org/10.1038/s41598-019-48956-x.
Krupp, R., 1988. Physicochemical aspects of mercury metallogenesis. Chem. Geol. 69, 345–356.
Kübler, B., 1964. Les argiles, indicateurs de métamorphisme. Rev. Inst. Francais Pétrole 19, 1093–1112 (in French).
Kübler, B., 1983. Dosage quantitatif des minéraux majeurs des roches sédimentaires par diffraction X. Cahiers de l'Institut de Géologie Series AX, pp. 1–13 (in French).
Kuroda, J., Hori, R.S., Suzuki, K., Gröcke, D.R., Ohkouchi, N., 2010. Marine osmium isotope record across the Triassic-Jurassic boundary from a Pacific pelagic site. Geology 38, 1095–1098.
Landoll, J.D., Foland, K., Henderson, C., 1989. Excess argon in amphiboles from fluid interaction and short intrusion interval at the epizonal Marangudzi complex, Zimbabwe. J. Geophys. Res. Solid Earth 94, 4053–4069.
Le Gall, B., Tshoso, G., Jourdan, F., Féraud, G., Bertrand, H., Tiercelin, J.-J., Kampunzu, A., Modisi, M., Dyment, J., Maia, M., 2002. 40Ar/39Ar geochronology and structural data from the giant Okavango and related mafic dyke swarms, Karoo igneous province, northern Botswana. Earth Planet. Sci. Lett. 202, 595–606.
Lena, L.F., Taylor, D., Guex, J., Bartolini, A., Adatte, T., van Acken, D., Spangenberg, J.E., Samankassou, E., Vennemann, T., Schaltegger, U., 2019. The driving mechanisms of the carbon cycle perturbations in the late Pliensbachian (Early Jurassic). Sci. Rep. 9. https://doi.org/10.1038/s41598-019-54593-1.
Littler, K., Hesselbo, S.P., Jenkyns, H.C.J.G.M., 2010. A carbon-isotope perturbation at the Pliensbachian–Toarcian boundary: evidence from the Lias Group, NE England. Geol. Mag. 147, 181–192.
Liu, X., Xu, L., Chen, Q., Sun, L., Wang, Y., Yan, H., Liu, Y., Luo, Y., Huang, J., 2012. Historical change of mercury pollution in remote Yongle archipelago, South China Sea. Chemosphere 87, 549–556.
McArthur, J.M., Donovan, D.T., Thirlwall, M.F., Fouke, B.W., Mattey, D., 2000. Strontium isotope profile of the early Toarcian (Jurassic) oceanic anoxic event, the duration of ammonite biozones, and belemnite palaeotemperatures. Earth Planet. Sci. Lett. 179, 269–285.
Macchioni, F., Cecca, F., 2002. Biodiversity and biogeography of middle–late Liassic ammonoids: implications for the early Toarcian mass extinction. Geobios 35, 165–175.
Marino, M., Santantonio, M., 2010. Understanding the geological record of carbonate platform drowning across rifted Tethyan margins: examples from the Lower Jurassic of the Apennines and Sicily (Italy). Sediment. Geol. 225, 116–137.
Martinez, M., Dera, G., 2015. Orbital pacing of carbon fluxes by a approximately 9-My eccentricity cycle during the Mesozoic. Proc. Natl. Acad. Sci. U.S.A. 112, 12604–12609.
Marzoli, A., Renne, P.R., Piccirillo, E.M., Ernesto, M., Bellieni, G., De Min, A., 1999. Extensive 200-million-year-old continental flood basalts of the Central Atlantic Magmatic Province. Science 284, 616–618.
Marzoli, A., Bertrand, H., Knight, K.B., Cirilli, S., Buratti, N., Vérati, C., Nomade, S., Renne, P. R., Youbi, N., Martini, R., Allenbach, K., Neuwerth, R., Rapaille, C., Zaninetti, L., Bellieni, G., 2004. Synchrony of the Central Atlantic magmatic province and the Triassic-Jurassic boundary climatic and biotic crisis. Geology 32 973–971.
Marzoli, A., Jourdan, F., Puffer, J.H., Cuppone, T., Tanner, L.H., Weems, R.E., Bertrand, H., Cirilli, S., Bellieni, G., De Min, A., 2011. Timing and duration of the Central Atlantic magmatic province in the Newark and Culpeper basins, eastern USA. Lithos 122, 175–188.
Mattioli, E., Erba, E., 1999. Synthesis of calcareous nannofossil events in Tethyan lower and middle Jurassic successions. Riv. Ital. Paleontol. Stratigr. 105, 343–376.
McHone, G.J., 1996. Broad-terrane Jurassic flood basalts across northeastern North America. Geology 24, 319–322.
Mercuzot, M., Pellenard, P., Durlet, C., Bougeault, C., Meister, C., Dommergues, J.-L., Thibault, N., Baudin, F., Mathieu, O., Bruneau, L., 2020. Carbon-isotope events during the Pliensbachian (Lower Jurassic) on the African and European margins of the NW Tethyan Realm. Newsl. Stratigr. 53, 41–69.
Moore, D.M., Reynolds, R.C., 1989. X-ray Diffraction and the Identification and Analysis of Clay Minerals. University Press, Oxford 322 pp.
Morettini, E., Santantonio, M., Bartolini, A., Cecca, F., Baumgartner, P., Hunziker, J., 2002. Carbon isotope stratigraphy and carbonate production during the Early–Middle Jurassic: examples from the Umbria–Marche–Sabina Kübler Apennines (central Italy). Palaeogeogr. Palaeoclimatol. Palaeoecol. 184, 251–273.
Mouterde, R., Ruget, C., 1975. Esquisse de la paléogéographie du Jurassique inférieur et moyen au Portugal. Bull. Soc. Geol. Fr. 7, 779–786 (in French).
Nesbitt, H.W., Young, G., 1982. Early Proterozoic climates and plate motions inferred from major element chemistry of lutites. Nature 299, 715–717.
Nesbitt, H., Young, G.M., 1989. Formation and diagenesis of weathering profiles. J. Geol. 97, 129–147.
Nomade, S., Knight, K., Beutel, E., Renne, P., Verati, C., Féraud, G., Marzoli, A., Youbi, N., Bertrand, H., 2007. Chronology of the Central Atlantic Magmatic Province: implications for the Central Atlantic rifting processes and the Triassic–Jurassic biotic crisis. Palaeogeogr. Palaeoclimatol. Palaeoecol. 244, 326–344.
Oliveira, L., Rodrigues, R., Duarte, L.V., Lemos, V., 2006. Avaliação do potencial gerador de petróleo e interpretação paleoambiental com base em biomarcadores e isótopos estáveis do carbono da seção Pliensbaquiano-Toarciano inferior (Jurássico inferior) da região de Peniche (Bacia Lusitânica, Portugal). Boletim de Geociências da Petrobras 14, 207–234 (in Portuguese).
Oliveira, L.C., Duarte, L.V., Silva, R.L., Rodrigues, R., 2009. Belemnite δ18O and δ13C record of the Lusitanian Basin Pliensbachian carbonate series (Portugal). Geochim. Cosmochim. Acta 73, A969.

Olsen, P.E., Kent, D.V., Et-Touhami, M., Puffer, J., 2003. Cyclo-, magneto-, and bio-stratigraphic constraints on the duration of the CAMP event and its relationship to the Triassic-Jurassic boundary. Geophys. Monogr. Ser. 136, 7–32.
Outridge, P., Sanei, H., Stern, G., Hamilton, P., Goodarzi, F., 2007. Evidence for control of mercury accumulation rates in Canadian High Arctic lake sediments by variations of aquatic primary productivity. Environ. Sci. 41, 5259–5265.
Pankhurst, R., Riley, T., Fanning, C., Kelley, S., 2000. Episodic silicic volcanism in Patagonia and the Antarctic Peninsula: chronology of magmatism associated with the break-up of Gondwana. J. Petrol. 41, 605–625.
Percival, L.M.E., Witt, M.L.I., Mather, T.A., Hermoso, M., Jenkyns, H.C., Hesselbo, S.P., Al-Suwaidi, A.H., Storm, M.S., Xu, W., Ruhl, M., 2015. Globally enhanced mercury deposition during the end-Pliensbachian extinction and Toarcian OAE: a link to the Karoo–Ferrar Large Igneous Province. Earth Planet. Sci. Lett. 428, 267–280.
Percival, L.M.E., Cohen, A.S., Davies, M.K., Dickson, A.J., Hesselbo, S.P., Jenkyns, H.C., Leng, M.J., Mather, T.A., Storm, M.S., Xu, W., 2016. Osmium isotope evidence for two pulses of increased continental weathering linked to Early Jurassic volcanism and climate change. Geology 44, 759–762.
Peti, L., Thibault, N., 2017. Abundance and size changes in the calcareous nannofossil Schizosphaerella – relation to sea-level, the carbonate factory and palaeoenvironmental change from the Sinemurian to earliest Toarcian of the Paris Basin. Palaeogeogr. Palaeoclimatol. Palaeoecol. 485, 271–282.
Peti, L., Thibault, N., Clémence, M.-E., Korte, C., Dommergues, J.-L., Bougeault, C., Pellenard, P., Jelby, M.E., Ullmann, C.V., 2017. Sinemurian–Pliensbachian calcareous nannofossil biostratigraphy and organic carbon isotope stratigraphy in the Paris Basin: calibration to the ammonite biozonation of NW Europe. Palaeogeogr. Palaeoclimatol. Palaeoecol. 468, 142–161.
Philippe, M., Thevenard, F., 1996. Distribution and palaeoecology of the Mesozoic wood genus Xenoxylon: palaeoclimatological implications for the Jurassic of Western Europe. Rev. Palaeobot. Palynol. 91, 353–370.
Philippe, M., Puijalon, S., Suan, G., Mousset, S., Thévenard, F., Mattioli, E., 2017. The palaeolatitudinal distribution of fossil wood genera as a proxy for European Jurassic terrestrial climate. Palaeogeogr. Palaeoclimatol. Palaeoecol. 466, 373–381.
Pirrone, N., Cinnirella, S., Feng, X., Finkelman, R.B., Friedli, H.R., Leaner, J., Mason, R., Mukherjee, A.B., Stracher, G.B., Streets, D., 2010. Global mercury emissions to the atmosphere from anthropogenic and natural sources. Atmos. Chem. Phys. Chem. Earth 10, 5951–5964.
Porter, S.J., Selby, D., Suzuki, K., Gröcke, D., 2013. Opening of a trans-Pangaean marine corridor during the Early Jurassic: Insights from osmium isotopes across the Sinemurian–Pliensbachian GSSP, Robin Hood's Bay, UK. Palaeogeogr. Palaeoclimatol. Palaeoecol. 375, 50–58.
Price, G.D., 1999. The evidence and implications of polar ice during the Mesozoic. Earth Sci. Rev. 48, 183–210.
Price, G.D., Twitchett, R.J., Wheeley, J.R., Buono, G., 2013. Isotopic evidence for long term warmth in the Mesozoic. Sci. Rep. 3, 1438. https://doi.org/10.1038/srep01438.
Price, G.D., Baker, S.J., VanDeVelde, J., Clémence, M.-E., 2016. High-resolution carbon cycle and seawater temperature evolution during the Early Jurassic (Sinemurian-Early Pliensbachian). Geochem. Geophys. Geosyst. 17, 3917–3928.
Pyle, D.M., Mather, T.A., 2003. The importance of volcanic emissions for the global atmospheric mercury cycle. Atmos. Environ. 37, 5115–5124.
Quesada, S., Robles, S., Rosales, I., 2005. Depositional architecture and transgressive–regressive cycles within Liassic backstepping carbonate ramps in the Basque–Cantabrian Basin, northern Spain. J. Geol. Soc. 162, 531–548.
Radley, J.D., 2008. Seafloor erosion and sea-level change: Early Jurassic Blue Lias Formation of central England. Palaeogeogr. Palaeoclimatol. Palaeoecol. 270, 287–294.
Renz, C., 1920. Beiträge zur Kenntnis der Juraformation im Gebiet des Monte Generoso (Kanton Tessin). Eclogae Geol. Helv. 15, 523–584 (in German).
Riley, T., Millar, I.L., Watkeys, M., Curtis, M.L., Leat, P., Klausen, M., Fanning, C., 2004. U–Pb zircon (SHRIMP) ages for the Lebombo rhyolites, South Africa: refining the duration of Karoo volcanism. J. Geol. Soc. 161, 547–550.
Riley, T., Curtis, M., Leat, P., Watkeys, M., Duncan, R., Millar, I., Owens, W., 2006. Overlap of Karoo and Ferrar magma types in KwaZulu-Natal, South Africa. J. Petrol. 47, 541–566.
Rogov, M., Zakharov, V., 2010. Jurassic and Lower Cretaceous glendonite occurrences and their implication for Arctic paleoclimate reconstructions and stratigraphy. Front. Earth Sci. 17 (Special issue), 345–346.
Rosales, I., Quesada, S., Robles, S., 2004a. Paleotemperature variations of Early Jurassic seawater recorded in geochemical trends of belemnites from the Basque–Cantabrian basin, northern Spain. Palaeogeogr. Palaeoclimatol. Palaeoecol. 203, 253–275.
Rosales, I., Robles, S., Quesada, S., 2004b. Elemental and oxygen isotope composition of Early Jurassic belemnites: salinity vs. temperature signals. J. Sediment. Res. 74, 342–354.
Rosales, I., Quesada, S., Robles, S., 2006. Geochemical arguments for identifying second-order sea-level changes in hemipelagic carbonate ramp deposits. Terra Nova 18, 233–240.
Rosales, I., Barnolas, A., Goy, A., Sevillano, A., Armendáriz, M., López-García, J.M., 2018. Isotope records (C-O-Sr) of late Pliensbachian-early Toarcian environmental perturbations in the westernmost Tethys (Majorca Island, Spain). Palaeogeogr. Palaeoclimatol. Palaeoecol. 497, 168–185.
Roth, P.H., 1984. Preservation of calcareous nannofossils and fine-grained carbonate particles in mid-Cretaceous sediments from the southern Angola Basin. Initial Reports of the Deep Sea Drilling Project 75. US Government Printing Office Washington, DC, pp. 651–655.
Royer, D.L., 2006. CO2-forced climate thresholds during the Phanerozoic. Geochim. Cosmochim. Acta 70, 5665–5675.
Ruebsam, W., Mayer, B., Schwark, L., 2019. Cryosphere carbon dynamics control early Toarcian global warming and sea level evolution. Glob. Planet. Chang. 172, 440–453.
Rühl, M., Hesselbo, S.P., Hinnov, L., Jenkyns, H.C., Xu, W., Riding, J.B., Storm, M., Minisini, D., Ullmann, C.V., Leng, M.J., 2016. Astronomical constraints on the duration of the Early Jurassic Pliensbachian Stage and global climatic fluctuations. Earth Planet. Sci. Lett. 455, 149–165.
Ruiz, W.L.G., Tomiyasu, T., 2015. Distribution of mercury in sediments from Kagoshima Bay, Japan, and its relationship with physical and chemical factors. Environ. Earth Sci. 74, 1175–1188.
Sabatino, N., Ferraro, S., Coccioni, R., Bonsignore, M., Del Core, M., Tancredi, V., Sprovieri, M., 2018. Mercury anomalies in upper Aptian-lower Albian sediments from the Tethys realm. Palaeogeogr. Palaeoclimatol. Palaeoecol. 495, 163–170.
Sanei, H., Grasby, S.E., Beauchamp, B., 2012. Latest Permian mercury anomalies. Geology 40, 63–66.
Schöllhorn, 2019. Climatic and Environmental Changes during the Early Jurassic: A Comparison between the Wessex, South German and Lombardian Basins. (Ph.D. thesis). University of Lausanne, Earth Sciences Institute, Switzerland.
Schöllhorn, I., Adatte, T., Houben, A., Van de Schootbrugge, B., Charbonnier, G., Janssen, N., Föllmi, K.B., 2020. Climate and environmental response to the break-up of Pangaea during the Hettangian-Pliensbachian; the Dorset coast (UK) revisited. Glob. Planet. Chang. 185, 103096. https://doi.org/10.1016/j.gloplacha.2019.103096.
Sell, B., Ovtcharova, M., Guex, J., Bartolini, A., Jourdan, F., Spangenberg, J.E., Vicente, J.-C., Schaltegger, U., 2014. Evaluating the temporal link between the Karoo LIP and climatic–biologic events of the Toarcian Stage with high-precision U–Pb geochronology. Earth Planet. Sci. Lett. 408, 48–56.
Silva, R.L., Duarte, L.V., 2015. Organic matter production and preservation in the Lusitanian Basin (Portugal) and Pliensbachian climatic hot snaps. Glob. Planet. Chang. 131, 24–34.
Silva, R.L., Duarte, L.V., Comas-Rengifo, M.J., Mendonça Filho, J.G., Azerêdo, A.C., 2011. Update of the carbon and oxygen isotopic records of the Early–Late Pliensbachian (Early Jurassic, ~187Ma): Insights from the organic-rich hemipelagic series of the Lusitanian Basin (Portugal). Chem. Geol. 283, 177–184.
Smith, P.L., 1983. The Pliensbachian ammonite Dayiceras dayiceroides and early Jurassic paleogeography. Can. J. Earth Sci. 20, 86–91.
Smith, P.L., Tipper, H.W., 1986. Plate tectonics and paleobiogeography: Early Jurassic (Pliensbachian) endemism and diversity. Palaios 1, 399–412.
Smith, P.L., Westermann, G.E., Stanley Jr., G.D., Yancey, T.E., Newton, C.R., 1990. Paleobiogeography of the ancient Pacific. Science 249, 680–683.
Speranza, F., Parisi, G., 2007. High-resolution magnetic stratigraphy at Bosso Stirpeto (Marche, Italy): Anomalous geomagnetic field behaviour during early Pliensbachian (early Jurassic) times? Earth Planet. Sci. Lett. 256, 344–359.
Steinthorsdottir, M., Vajda, V., 2013. Early Jurassic (late Pliensbachian) CO2 concentrations based on stomatal analysis of fossil conifer leaves from eastern Australia. Gondwana Res. 27, 932–939.
Stockar, R., 2003. The Breggia Gorge Park. Parco delle Gole della Breggia. Morbio Inferiore, Switzerland.
Suan, G., Mattioli, E., Pittet, B., Mailliot, S., Lécuyer, C., 2008. Evidence for major environmental perturbation prior to and during the Toarcian (Early Jurassic) oceanic anoxic event from the Lusitanian Basin, Portugal. Paleoceanography 23. https://doi.org/10.1029/2007PA001459.
Suan, G., Mattioli, E., Pittet, B., Lécuyer, C., Suchéras-Marx, B., Duarte, L.V., Philippe, M., Reggiani, L., Martineau, F., 2010. Secular environmental precursors to Early Toarcian (Jurassic) extreme climate changes. Earth Planet. Sci. Lett. 290, 448–458.
Suan, G., Schöllhorn, I., Schlögl, J., Segit, T., Mattioli, E., Lécuyer, C., Fourel, F., 2018. Euxinic conditions and high sulfur burial near the European shelf margin (Pieniny Klippen Belt, Slovakia) during the Toarcian oceanic anoxic event. Glob. Planet. Chang. 170, 246–259.
Surlyk, F., 2003. The Jurassic of Denmark and Greenland: the Jurassic of East Greenland: a sedimentary record of thermal subsidence, onset and culmination of rifting. Geol. Surv. Den. Greenl. 1, 659–722.
Svensen, H., Corfu, F., Polteau, S., Hammer, Ø., Planke, S., 2012. Rapid magma emplacement in the Karoo large igneous province. Earth Planet. Sci. Lett. 325, 1–9.
Teichert, B.M.A., Luppold, F.W., 2013. Glendonites from an Early Jurassic methane seep — climate or methane indicators? Palaeogeogr. Palaeoclimatol. Palaeoecol. 390, 81–93.
Thibodeau, A.M., Ritterbush, K., Yager, J.A., West, A.J., Ibarra, Y., Bottjer, D.J., Berelson, W. M., Bergquist, B.A., Corsetti, F.A. , 2016. Mercury anomalies and the timing of biotic recovery following the end-Triassic mass extinction. Nat. Commun. 7, 11147. https://doi.org/10.1038/ncomms11147.
Thierry, J.M.T., 2000. map 8. In: Dercourt, J., Gaetani, M., Barrier, E., Biju-Duval, B., Brunet, M.F., Crasquin, S., Sandulescu, M. (Eds.), Atlas Peri-, Tethys Palaeogeographical Maps Commission for the Geological Map of the World, Paris, pp. 61–70.
Trecalli, A., Spangenberg, J., Adatte, T., Föllmi, K.B., Parente, M.J.E., Letters, P.S., 2012. Carbonate platform evidence of ocean acidification at the onset of the early Toarcian oceanic anoxic event. Earth Planet. Sci. Lett. 357, 214–225.
Val, J., Bádenas, B., Aurell, M., Rosales, I., 2017. Cyclostratigraphy and chemostratigraphy of a bioclastic storm-dominated carbonate ramp (late Pliensbachian, Iberian Basin). Sediment. Geol. 355, 93–113.
Van Buchem, F., Melnyk, D., McCave, I., 1992. Chemical cyclicity and correlation of Lower Lias mudstones using gamma ray logs, Yorkshire, UK. J. Geol. Soc. 149, 991–1002.
van de Schootbrugge, B., Bailey, T.R., Rosenthal, Y., Katz, M.E., Wright, J.D., Miller, K.G., Feist-Burkhardt, S., Falkowski, P.G., 2005. Early Jurassic climate change and the radiation of organic-walled phytoplankton in the Tethys Ocean. Paleobiology 31, 73–97.
van de Schootbrugge, B., Harazim, D., Sorichter, K., Oschmann, W., Fiebig, J., Püttmann, W., Peinl, M., Zanella, F., Teichert, B.M.A., Hoffmann, J., Stadnitskaia, A., Rosenthal, Y., 2010. The enigmatic ichnofossil Tisoa siphonalis and widespread authigenic seep carbonate formation during the Late Pliensbachian in southern France. Biogeosciences 7, 3123–3138.

Venturi, F., Bilotta, M., Ricci, C., 2006. Comparison between western Tethys and eastern Pacific ammonites: further evidence for a possible late Sinemurian–early Pliensbachian trans-Pangaean marine connection. Geol. Mag. 143, 699–711.

Venturi, F., Nannarone, C., Bilotta, M., 2007. Ammonites from the early Pliensbachian of the Furlo Pass (Marche, Italy): biostratigraphic and paleobiogeographic implications. Boll. Soc. Paleontol. Ital. 46, 1–31.

Verati, C., Rapaille, C., Féraud, G., Marzoli, A., Bertrand, H., Youbi, N., 2007. 40Ar/39Ar ages and duration of the Central Atlantic Magmatic Province volcanism in Morocco and Portugal and its relation to the Triassic–Jurassic boundary. Palaeogeogr. Palaeoclimatol. Palaeoecol. 244, 308–325.

Wang, Y., Mosbrugger, V., Zhang, H., 2005. Early to Middle Jurassic vegetation and climatic events in the Qaidam Basin, Northwest China. Palaeogeogr. Palaeoclimatol. Palaeoecol. 224, 200–216.

Warrington, G., Ivimey-Cook, H.C., 1995. The late Triassic and early Jurassic of coastal sections in west Somerset and South and Mid-Glamorgan. In: Taylor, P.D. (Ed.), Field Geology of the British Jurassic, The Geological Society, London, pp. 9–30.

White, L.T., Ireland, T.R., 2012. High-uranium matrix effect in zircon and its implications for SHRIMP U–Pb age determinations. Chem. Geol. 306, 78–91.

Whiteside, J.H., Olsen, P.E., Kent, D.V., Fowell, S.J., Et-Touhami, M., 2007. Synchrony between the Central Atlantic magmatic province and the Triassic–Jurassic mass-extinction event? Palaeogeogr. Palaeoclimatol. Palaeoecol. 244, 345–367.

Wiedenmayer, F., 1980. Die Ammoniten der mediterranen Provinz im Pliensbachian und unteren Toarcian aufgrund neuer Untersuchungen im Generoso-Becken (Lombardische Alpen). (Ph.D. thesis). University of Glarus/Zürich 192 pp. (in German).

Wignall, P.B., Newton, R., Brookfield, M.E., 2005. Pyrite framboid evidence for oxygen-poor deposition during the Permian–Triassic crisis in Kashmir. Palaeogeogr. Palaeoclimatol. Palaeoecol. 216, 183–188.

Williams, I., Hergt, J.M., 2000. U-Pb dating of Tasmanian dolerites: a cautionary tale of SHRIMP analysis of high-U zircon. In: Woodhead, J.D., Hergt, J.M., Noble, W.P. (Eds.), Beyond 2000: New Frontiers in Isotope Geoscience. Lorne, Australia, pp. 185–188.

Winterer, E.L., Bosellini, A., 1981. Subsidence and sedimentation on Jurassic passive continental margin, Southern Alps, Italy. AAPG Bull. 65, 394–421.

Woodfine, R.G., Jenkyns, H.C., Sarti, M., Baroncini, F., Violante, C., 2008. The response of two Tethyan carbonate platforms to the early Toarcian (Jurassic) oceanic anoxic event: environmental change and differential subsidence. Sedimentology 55, 1011–1028.

Xu, W., Mac Niocaill, C., Ruhl, M., Jenkyns, H.C., Riding, J.B., Hesselbo, S.P., 2018. Magnetostratigraphy of the Toarcian Stage (Lower Jurassic) of the Llanbedr (Mochras Farm) Borehole, Wales: basis for a global standard and implications for volcanic forcing of palaeoenvironmental change. J. Geol. Soc. 175, 594–604.

Zhang, X., Luttinen, A., Elliot, D., Larsson, K., Foland, K., 2003. Early stages of Gondwana breakup: the 40Ar/39Ar geochronology of Jurassic basaltic rocks from western Dronning Maud Land, Antarctica, and implications for the timing of magmatic and hydrothermal events. J. Geophys. Res. Solid Earth 108. https://doi.org/10.1029/2001JB001070.